Study of neutrino-nucleus interaction at around 1 GeV using a 3D grid-structure neutrino detector, WAGASCI, muon range detectors and magnetized spectrometer, Baby MIND, at J-PARC neutrino monitor hall

A. Bonnemaison, R. Cornat, L. Domine, O. Drapier, O. Ferreira, F. Gastaldi, M. Gonin, J. Imber, M. Licciardi, F. Magniette, T. Mueller, L. Vignoli, and O. Volcy

Ecole Polytechnique, IN2P3-CNRS, Laboratoire Leprince-Ringuet, Palaiseau, France

S. Cao and T. Kobayashi

High Energy Accelerator Research Organization (KEK), Tsukuba, Ibaraki, Japan

M. Khabibullin, A. Khotjantsev, A. Kostin, Y. Kudenko, A. Mefodiev, O. Mineev, S. Suvorov, and N. Yershov

Institute for Nuclear Research of the Russian Academy of Sciences, Moscow, Russia

B. Quilain

Kavli Institute for the Physics and Mathematics of the Universe (WPI), The University of Tokyo Institutes for Advanced Study, University of Tokyo, Kashiwa, Chiba, Japan

T. Hayashino, A. Hiramoto, A.K. Ichikawa, K. Nakamura, T. Nakaya, K Yasutome, and K. Yoshida

Kyoto University, Department of Physics, Kyoto, Japan

Y. Azuma, J. Harada, T. Inoue, K. Kin, N. Kukita, S. Tanaka, Y. Seiya, K. Wakamatsu, and K. Yamamoto

Osaka City University, Department of Physics, Osaka, Japan

A. Blondel, F. Cadoux, Y. Favere, E. Noah, L. Nicola, and S. Parsa

University of Geneva, Section de Physique, DPNC, Geneva, Switzerland

N. Chikuma, F. Hosomi, T. Koga, R. Tamura, and M. Yokoyama

University of Tokyo, Department of Physics, Tokyo, Japan

Y. Hayato

University of Tokyo, Institute for Cosmic Ray Research, Kamioka Observatory, Kamioka, Japan

Y. Asada, K. Matsushita, A. Minamino, K. Okamoto, and D. Yamaguchi

Yokohama National University, Faculty of Engineering, Yokohama, Japan

December 14, 2017

Contents

1 Introduction

The understanding of neutrino-nucleus interactions in the 1 GeV energy region is critical for the success of accelerator-based neutrino oscillation experiments such as the T2K experiment. Complicated multi-body effects of nuclei render this understanding difficult. The T2K near detectors have been measuring these and significant progress has been achieved. However, the understanding is still limited. One of the big factors preventing from full understanding is the non-monochromatic neutrino beam spectrum. Measurements with different but some overlapping beam spectra would greatly benefit to resolve the contribution from different neutrino energies. We, the Wagasci collaboration, proposes to study the neutrino-nucleus interaction at the B2 floor of the neutrino monitor building, where different neutrino spectra can be obtained due to the different off-axis position. Our experimental setup contains 3D grid-structure plastic-scintillator detectors filled with water as the neutrino interaction target (Wagasci modules), two side- and one downstream- muon range detectors(MRD's). The 3D grid-structure and side-MRD's allows a measurement of wider-angle scattering than the T2K off-axis near detector (ND280). High water to scintillator material ratio enables the measurement of the neutrino interaction on water, which is highly desired for the T2K experiment because it's far detector, Super-Kamiokande, is composed of water. The MRD's consist of plastic scintillators and iron plates. The downstream-MRD, so called the Baby MIND detector, also works as a magnet and provides the charge identification capability as well as magnetic momentum measurement for high energy muons. The charge identification is essentially important to select antineutrino events in the antineutrino beam because contamination of the neutrino events is as high as 30%. Most of the detectors has been already constructed. The Wagasci modules have been commissioned as the J-PARC T59 experiment and the Baby MIND detector was commissioned at the CERN neutrino platform. Therefore, the collaboration will be ready to proceed to the physics data taking for the T2K beam time in January 2019. We will provide the cross sections of the charged current neutrino and antineutrino interactions on water with slightly higher neutrino energy than T2K ND280 with wide angler acceptance. When combined with ND280 measurements, our measurement would greatly improve the understanding of the neutrino interaction at around 1 GeV and contribute to reduce one of the most significant uncertainty of the T2K experiment.

2 Experimental Setup

Figure. 1 and 2 show a schematic view and a CAD drawing of the entire set of detectors. Central neutrino target detectors consist of two Wagasci modules and T2K INGRID proton module. Inside the Wagasci module, plastic scintillator bars are aligned as a 3D grid-like structure and spaces in the structure are filled with water for a water-in Wagasci module. T2K INGRID proton module is a full active neutrino target detector which is composed only with scintillator bars in its tracking region. The central detectors are surrounded by two side- and one downstream- muon range detectors(MRD's) The MRD's are used to select muon tracks from the charged-current (CC) interactions and to reject short tracks caused by neutral particles that originate mainly from neutrino interactions in material surrounding the central detector, like the walls of the detector hall, neutrons and gammas, or neutral-current (NC) interactions. The muon momentum can be reconstructed from its range inside the detector. The MRD's consist of plastic scintillators and iron plates. In addition, each of the iron plates of the downstream-MRD, so called the Baby MIND detector, is wound by a coil and can be magnetized. It provide the charge selection capability.

For all detectors, scintillation light in the scintillator bar is collected and transported to a photodetector with a wavelength shifting fiber (WLS fiber). The light is read out by a photodetector, Multi-Pixel Photon Counter (MPPC), attached to one end of the WLS fiber. The signal from the MPPC is read out by the dedicated electronics developed for the test experiment to enable bunch separation in the beam spill. The readout electronics is triggered using the beam-timing signal from MR to synchronize to the beam. The beam-timing signal is branched from those for T2K, and will not cause any effect on the T2K data taking.

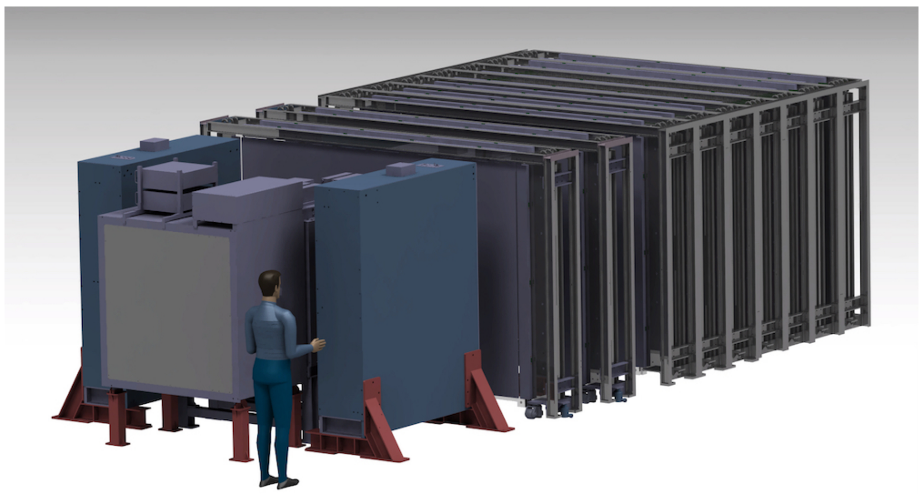

Figure 1: Schematic view of entire sets of detectors.

T2K adopted the off-axis beam method, in which the neutrino beam is intentionally directed 2.5 degrees away from SK producing a narrow band ν_μ beam. The off-axis near detector, ND280, is installed towards the SK direction in the B1 floor of the near detector hall of the J-PARC neutrino beam-line. We propose to install our detector in the B2 floor of the near detector hall, where the off-axis angle is similar but slightly different: 1.5 degree. The candidate detector position in the B2 floor is shown in Fig. 3. The expected neutrino energy spectrum at the candidate position is shown in Fig. 4.

2.1 Wagasci modules

2.1.1 Detector

The WAGASCI modules are mainly composed of 1280 plastic scintillator bars and a surrounding stainless steel tank as shown in Fig. 5. The total number of channels in one Wagasci module is 1280. The stainless steel tank is constructed by welding stainless steel plates, is sized as $46\times125\times125$ cm^3, and weighs 0.5 ton.

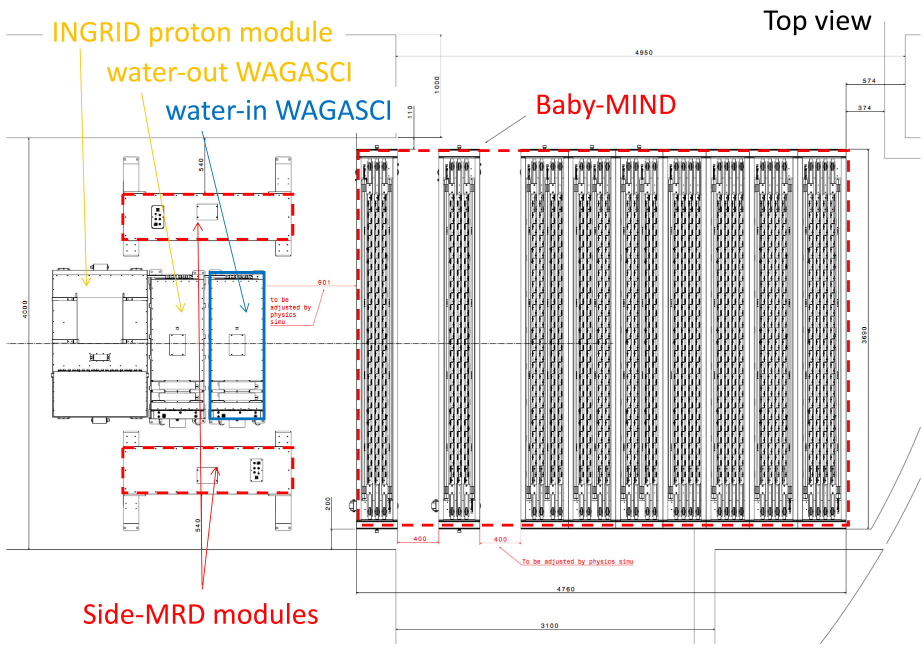

Figure 2: Top view of entire sets of detectors.

One Wagasci module consists of 16 scintillator tracking planes, where each plane is an array of 80 scintillator bars fixed with ABS frames. The 40 bars, called parallel scintillators, are placed perpendicularly to the beam, and the other 40 bars, called grid scintillators, are placed in parallel to the beam with grid structure in the tracking plane as shown in Fig. 5. Thanks to the 3 D grid-like structure of the scintillator bars, the Wagasci module has 4π angular acceptance for charged particles.

Thin plastic scintillator bars produced at Fermilab by extrusion method, mainly consists of polystyrene and are surrounded by thin reflector including TiO^2 (3 mm in thickness) are used for the Wagasci modules to reduce the mass ratio of scintillator bars to water, because neutrino interactions in the scintillator bars are a background for the cross section measurements on H_2O. Each scintillator bar is sized as $1020\times25\times3$ mm^3 including the reflector part, and half of all the scintillator bars have 5-cm-interval slits to form the grid structure (Figure 6).

We will have two types of the Wagasci modules, a water-in module and a water-out module. The water-in Wagasci module has water in spaces of the grid structure. The total water mass serving as neutrino targets in the fiducial volume of the module is 188 kg, and the mass ratio of scintillator bars to water is 80 %. The water-out Wagasci module doesn't have water inside the detector. The total CH mass serving as neutrino target in the fiducial

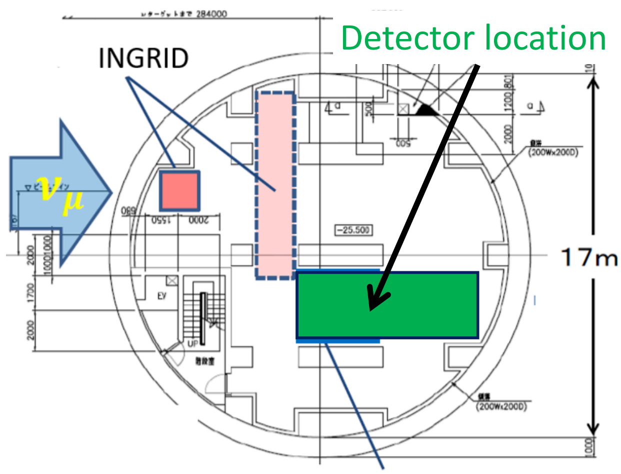

Figure 3: Candidate detector position in the B2 floor of the near detector hall.

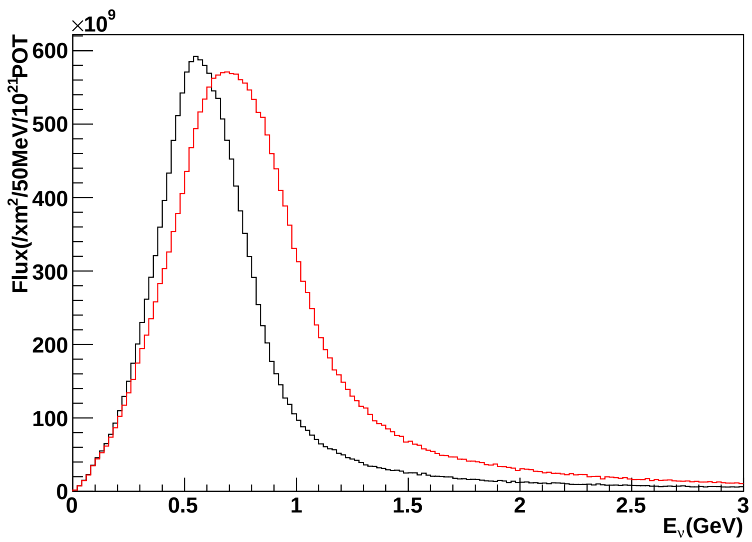

Figure 4: Neutrino energy spectrum at the candidate detector position(red, off-axis 1.5 degree). The spectrum at the ND280 site (black, off-axis 2.5 degree) is also shown.

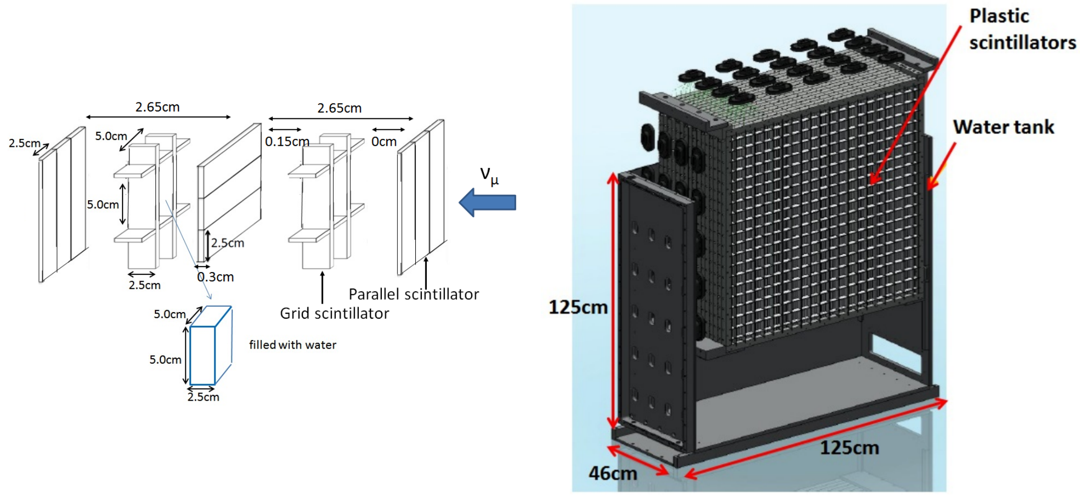

Figure 5: Schematic views of 3D grid-like structure of plastic scintillator bars (left) and Wagasci module (right).

volume of the module is 47 kg, and the mass fraction of scintillator bars is 100 %.

Scintillation light is collected by wave length shifting fibers, Y-11 (non-S type with a diameter of 1.0 mm produced by Kuraray. A fiber is glued by optical cement in a groove on surface of a scintillator bar. 32 fibers are gathered together by a fiber bundle at edge of the module, and lead scintillation light to a 32-channel arrayed MPPC. Since crosstalk of light yield due to reflection on the inner surface of each cell has been observed, all the scintillator bars are painted black by aqueous color spray. It is confirmed by measurements with cosmic rays that black painting on the surface of the scintillator bars suppresses this crosstalk so that no significant crosstalk effect is observed within uncertainty.

32-channel arrayed MPPCs, as shown in the Fig. 7, are used for the modules. The surface of the fiber bundle is polished and directly attached onto the 32-channel arrayed MPPCs. The positions of 32 fibers on the bundle are aligned to fit the channels of MPPCs. The MPPC is a product of Hamamatsu Photonics, S13660(ES1), with suppressed noise rate of $\sim$6 kHz per channel at 0.5 p.e. threshold. For each MPPC channel, 716 pixels of APD are aligned in a shape of circle.

2.1.2 Electronics

As front-end electronics of this detector, a Silicon PM Integrated Read-Out Chip (SPIROC) [10] is adopted. SPIROC is a 36-channel auto-triggered front-end ASIC, and is produced by OMEGA/ IN2P3. It not only contains an analog signal processing part such as amplification and shaping of the waveform, but contains a digital signal processing parts such as

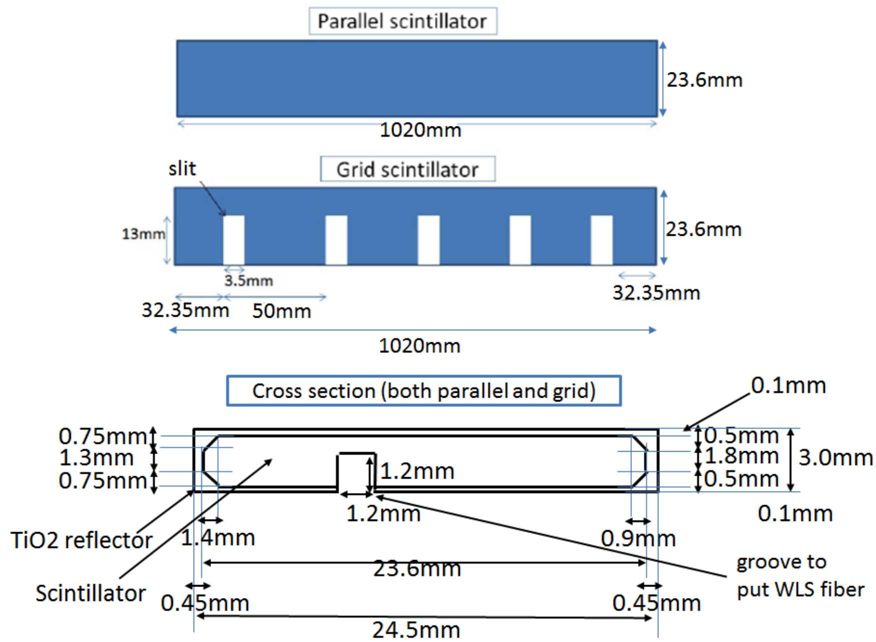

Figure 6: Geometry of scintillators used for Wagasci modules.

auto-trigger and timing measurement. Charge of MPPC signal is sampled by track-and-hold circuit. A Front-end electronics board, Active Sensor Unit (ASU), has been developed with the SPIROC2D chip, which is the latest version of SPIROC. Each readout board is designed to control a 32-channel arrayed MPPC, and 40 of the ASU boards are aligned on the module surface. The data acquisition system used for this detector, including back-end boards, has been developed for prototypes of ultra-granular calorimeters for the International Linear Collider (ILC) [4], and independent of the T2K DAQ system. To synchronize the DAQ system to J- PARC neutrino beam, pre-beam trigger and beam trigger are sent to the clock control card. The beam trigger signals are converted from optical signals to NIM signals at NIM module on the B2 floor. In addition, the information of spill number are delivered with 16-bit ECL level signals, and converted to an Ethernet frame by an FPGA evaluation board to be directly sent to the DAQ PC. The electronics readout scheme is shown in Fig. 8.

2.1.3 Water system

Pure water is filled to the water tank of the water-in Wagasci module as follows. First, the water storage tank located at the B2 floor of the NM pit is filled with water delivered from a water tap on the ground level through a long hose. Second, the water is pumped

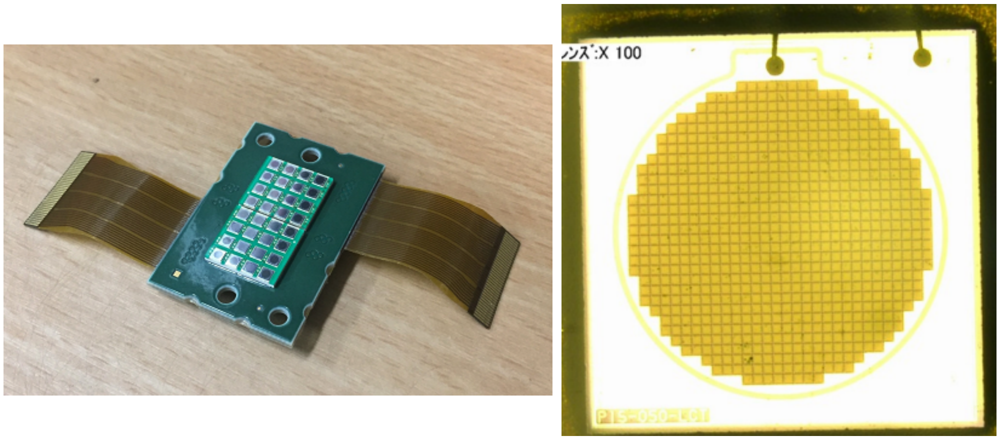

Figure 7: 32-channel arrayed MPPC (left) and an enlarged view of one MPPC channel (right).

to the other water storage tank though a water filler to produce pure water. Third, a compound preservative called Germall plus, which is the same preservative used in one of the sub-detectors of T2K ND280, FGD2, is put into the water to keep water from being bad. Then, the water is poured to the water-in Wagasci module, and it is kept in the module during the neutrino beam operation and not to be circulated.

2.2 INGRID Proton module

INGRID Proton module is a neutrino detectors of the T2K experiment. It is a fully-active tracking detector which consists of only scintillator strips. The purpose of this Proton Module is to separate the neutrino interaction types by detecting the protons and pions together with the muons from the neutrino interactions, and to measure the neutrino cross section for each interaction type. It consists of 36 tracking planes surrounded by veto planes (Figure 9), where each tracking plane is an array of two types of scintillator strips. The 16 strips in the inner region have dimensions of 2.5cm$\times$1.3cm$\times$120cm, while the 16 strips in the outer region have dimensions of 5cm$\times$1cm$\times$120cm, making a plane of 120$\times$120cm^2 in the horizontal and vertical directions. The former is the scintillator produced for the K2K SciBar detector [3] and the latter was produced for INGRID. The tracking planes are placed perpendicular to the beam axis at 23mm intervals. Since the strips are aligned in one direction, each tracking plane is sensitive to either the horizontal or vertical position of the tracks. The tracking planes are therefore placed alternating in the horizontal and vertical directions so that three-dimensional tracks can be reconstructed. The tracking planes also serve as the neutrino interaction target. As with the Wagasci modules, scintillation light is read out by a WLS fiber and MPPC.

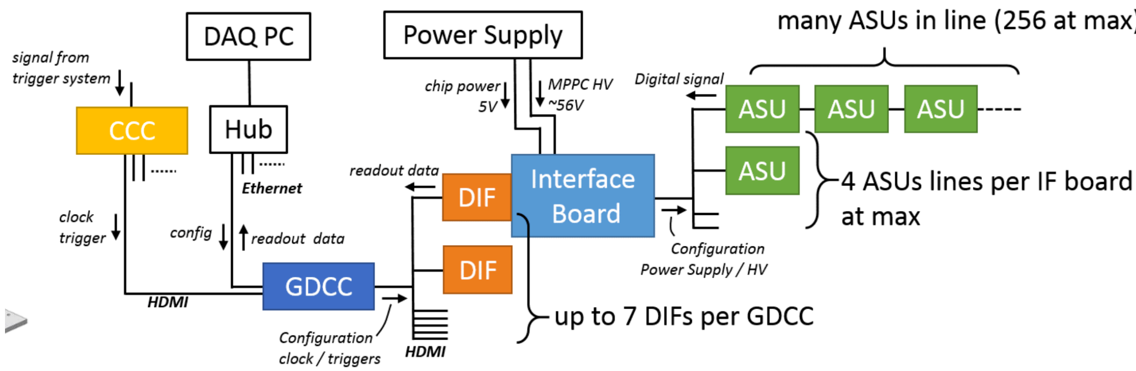

Figure 8: Wagasci electronics readout scheme.

It was installed at the neutrino beam axis on the SS floor of the T2K near detector hall in 2010, and had been used for neutrino cross section measurements. In August 2017, it was moved to the B2 floor of the T2K near detector hall by J-PARC T59 after getting the approval from T2K to use them. J-PARC T59 is performing a neutrino beam measurement using the detector from October 2017, and the measurement will continue until May 2018 as we will discuss in Sec. 4.

We will operate the INGRID Proton module using the T2K near detector electronics/DAQ system in the same way as J-PARC T59. A proposal to use the module and its electronics for our project will be submitted to the T2K collaboration.

2.3 Baby MIND

The Baby MIND is the downstream Muon Range Detector. It also works as a magnet and provides the charge identification capability as well as magnetic momentum measurement for high energy muons.

The Baby MIND collaboration [1] submitted a proposal to the SPSC at CERN, SPSC-P-353. The project was approved by the CERN research board as Neutrino Platform project NP05 and constructed. The detector consists of 33 magnet modules, each 3500 mm $\times$ 2000 mm$\times$ 50 mm (30 mm steel) with a mass of approximately 2 tonnes. Of these magnet modules, 18 are instrumented with plastic scintillator modules.

2.3.1 Magnet modules

The Baby MIND is built from sheets of iron interleaved with scintillator detector modules but unlike traditional layouts for magnetized iron neutrino detectors (e.g. MINOS) which tend to be monolithic blocks with a unique pitch between consecutive steel segments and

[1] Contact person: E. Noah, Spokesperson: A. Blondel, Deputy spokesperson: Y. Kudenko

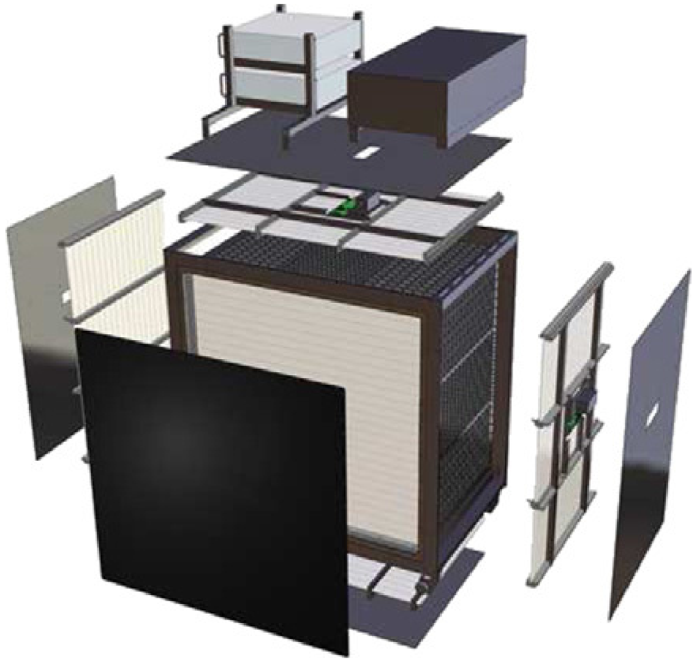

Figure 9: Schematic view of INGRID Proton module.

large conductor coils threaded around the whole magnet volume, the Baby MIND iron segments are all individually magnetized as shown inf Fig. 10, allowing for far greater flexibility in the setting of the pitch between segments, and in the allowable geometries that these detectors can take.

The key design outcome is a highly optimized magnetic field map. A double-slit configuration for coil winding was adopted to increase the area over which the magnetic flux lines are homogeneous in B_x across the central tracking region. Simulations show the magnet field map to be very uniform over this central tracking region covering an area of 2800×2000 mm^2, Fig. 11. The B_x component dominates in this region, with negligible B_y and B_z. This was confirmed by measuring the field with 9 pick-up coils wound around the first module. Subsequent modules were equipped with one pick-up coil. Test results on the 33 modules show all to achieve the required field of 1.5 T for a current of 140 A, with a total power consumption of 11.5 kW. The polarity of the field map shown in Fig. 11 (middle) can be reversed by changing the power supply configuration.

2.3.2 Scintillator modules

Each of the 18 scintillator modules is constructed from 2 planes of horizontal counters (95 counters in total) and 2 planes of vertical counters (16 counters in total) [2], arranged

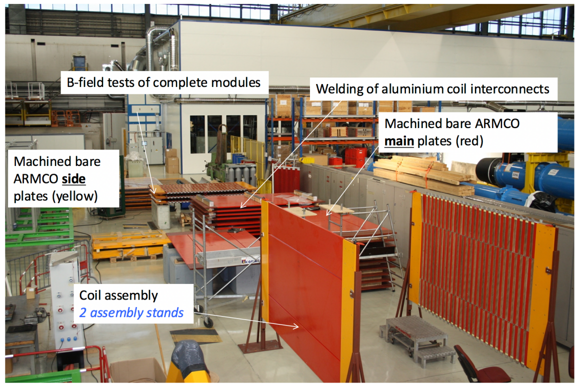

Figure 10: Magnet assembly zone at CERN.

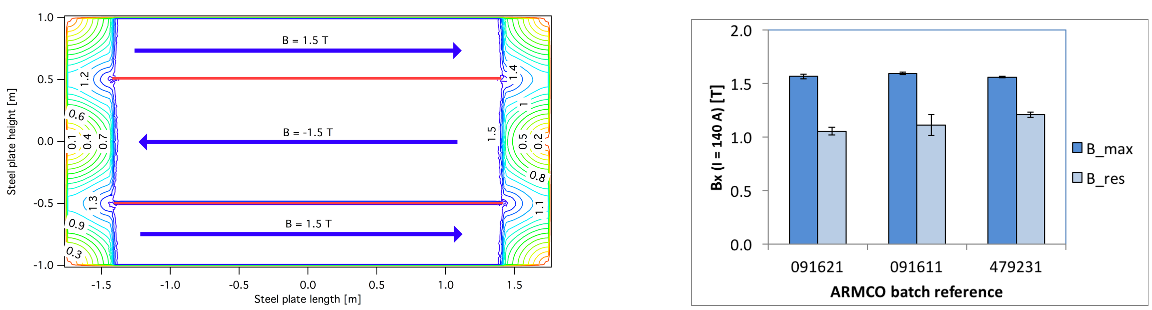

Figure 11: Left) Magnetic field map with a coil along 280 cm of the length of the plate. Right) Measured B field for 33 modules.

with an overlap between planes to achieve close to 100% hit efficiency for minimum ionizing muons. The arrangement of planes within a module is vertical-horizontal-horizontal-vertical. This arrangement was the result of an assembly approach whereby each plane was built from 2 half-planes, with each half plane consisting of a horizontal plane and a vertical plane. The scintillator bars are held in place using structural ladders that align and maintain the counters, Fig. 12. No glue is used in the process, so counters can be replaced. Aluminum sheets front and back provide light tightness.

Figure 12: Scintillator modules assembly. Left) top of front half-module showing vertical counters, and the spacers-ladders that set the pitch between horizontal counters and hold them in place. Middle) rear half-module showing horizontal counters on their ladders. Right) Assembled rear half-module, the front half-module can be seen in the background.

The plastic scintillator counters were made from 220 mm-wide slabs, consisting of extruded polystyrene doped with 1.5% paraterphenyl (PTP) and 0.01% POPOP. They were cut to size then covered with a 30-100 μm thick diffuse reflector resulting from etching of the surface with a chemical agent [7, 8]. The horizontal counter size is $2880 \times 31 \times 7.5$ mm^3, with one groove along the length of the bar in which sits a wavelength shifting fiber from Kuraray. The vertical counter size is $1950 \times 210 \times 7.5$ mm^3, with one U-shaped groove along the bar. On each counter, two custom connectors house silicon photomultipliers, MPPC type S12571-025C from Hamamatsu, either side of the horizontal counter, and both connectors at the top for the vertical counter. This geometrical configuration for vertical counters was chosen for ease of connectivity to the electronics, and maintenance operations.

A total of 1744 horizontal counters and 315 vertical counters (including spares) were produced at the Uniplast company (Vladimir, Russia).

2.3.3 Electronics

The Baby MIND electronic readout scheme includes several custom-designed boards [9]. The revised version is shown in Fig. 13. At the heart of the system is the electronics Front End Board (FEB), developed by the University of Geneva. The readout system includes two ancillary boards, the Backplane, and the Master Clock Board (MCB) whose development has been managed by INRNE (Bulgarian Academy of Sciences) collaborators.

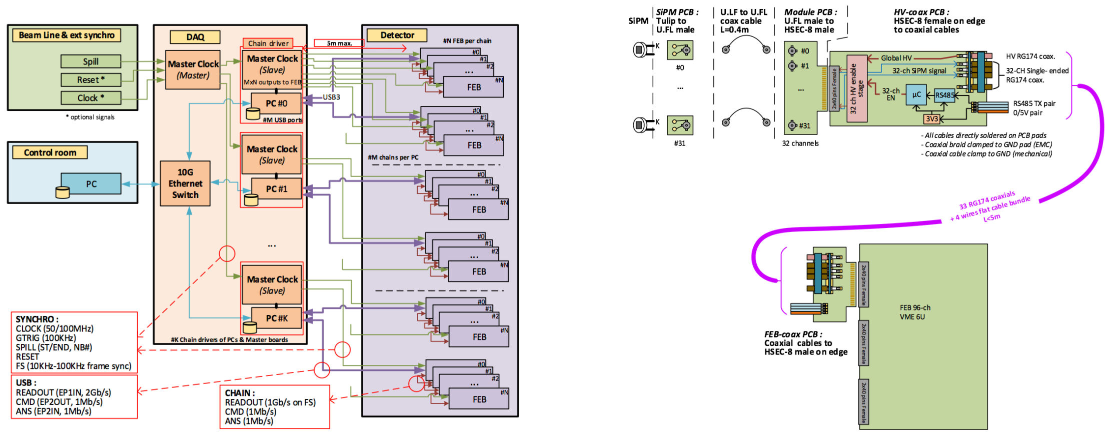

Figure 13: Left) Baby MIND electronics readout scheme. Right) SiPM-to-FEB connectivity.

The FEBv2 hosts 3 CITIROC chips that can each read in signals from 32 SiPMs [5]. Each signal input is processed by a high gain, and a separate low gain, signal path. The outputs from the slow shapers can be sampled using one of two modes: a mode with an externally applied delay, and a peak detector mode. A faster shaper can be switched to either HG or LG paths, followed by discriminators with adjustable thresholds providing 32 individual trigger outputs and one OR32 trigger output. An Altera ARIA5 FPGA on the FEBv2 samples these trigger outputs at 400 MHz, recording rising and falling times for the individual triggers and assigning time stamps to these. Time-over-threshold from the difference between falling and rising times gives some measure of signal amplitude, used in addition to charge information and useful if there is more than one hit per bar within the deadtime due to the readout of the multiplexed charge output of ~ 9 μs. The ARIA5 also manages the digitization of the sampled CITIROC multiplexed HG and LG outputs via a 12-bit 8-ch ADC.

The internal 400 MHz clock on the FEBv2 can be synchronized to a common 100 MHz clock. The synchronization subsystem combines input signals from the beam line into a digital synchronization signal (SYNC) and produces a common detector clock (CLK) which can eventually be synchronised to an external experiment clock. Both SYNC and CLK signals are distributed to the FEBs. Tests show the FEB-to-FEB CLK(SYNC) delay difference to be 50 ps (70 ps). Signals from the beam line at WAGASCI include two separate timing signals, arriving 100 ms and 30 μs before the neutrino beam at the near detectors. The spill number is available as a 16-bit signal.

2.3.4 Pefromance check

All counters were measured at INR Moscow with a cosmic ray setup using the same type S12571-025C MPPCs and CAEN DT5742 digitizer.The average light yield (sum from both ends) was measured to be 37.5 photo-electrons (p.e.) per minimum ionizing particle (MIP) and 65 p.e./MIP for vertical and horizontal counters, respectively. After shipment to CERN, all counters were tested once more individually with an LED test setup [?]. 0.1% of counters failed the LED tests and were therefore not used during the assembly of modules. The assembly of modules was completed in June 2017, and it was then tested in June and July 2017 at the Proton Synchrotron experimental hall at CERN with a mixed particle beam comprising mostly muons whose momenta could be selected between 0.5 and 5 GeV/c. An event display from the summer 2017 tests is shown in Fig. 14.

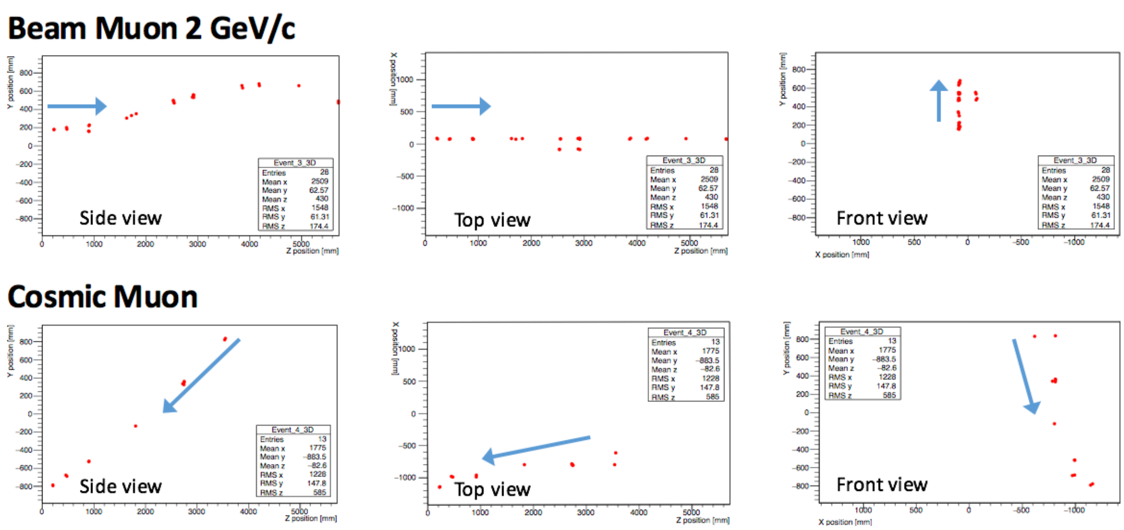

Figure 14: Comparison of a beam muon and cosmic muon in the three different geometrical projections of the detector. The beam impinges on the detector from the left. The arrows indicate the direction of travel of these muons. The direction of the cosmic muon is inferred from timing information.

2.4 Side muon range detector

Two Side-MRD modules for tracking secondary particles from neutrino interactions will be installed in 2018. Each Side-MRD module is composed of 11 steel plates and 10 layers of total 80 scintillator slabs installed in 13 mm gaps between the 30 mm thick plates. Each steel plate size is $30 \times 1610 \times 1800$ mm^3. Total module size is $2236 \times 1630 \times 975$ mm^3 as shown in Fig. 15 (left), weight is $\sim$8.5 ton.

Scintillator bars were manufactured by Uniplast company in Vladimir, Russia. Polystyrene based scintillators were extruded with thickness of 7 mm, then cut to the size of $7 \times 200 \times 1800$ mm^3. Dopant composition is 1.5% PTP and 0.01% POPOP. Scintillator surface was etched by a chemical agent to form a white diffuse layer with excellent reflective performance. Ideal contact between the scintillator and the reflector raises the light yield up to 50% comparing to an uncovered scintillator. Sine like groove was milled along the scintillator to provide uniform light collection over the whole scintillator surface. WLS Y11 Kuraray fiber of 1 mm diameter is glued with an optical cement EJ-500 in the S-shape groove as shown in Fig. 15(right). Bending radius is fixed to 30 mm that was specified to be safe for Kuraray S-type fibers. Both ends of the fiber are glued into optical connectors which mounted within a scintillator body and provide an interface to SiPMs, Hamamatsu MPPC S13081-050CS(X1).

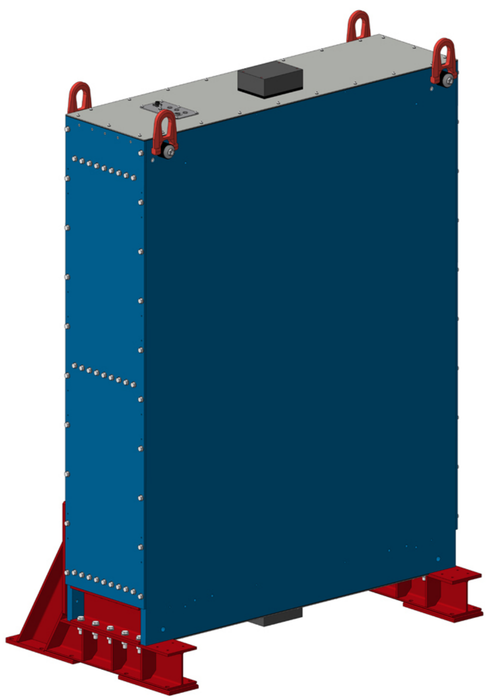

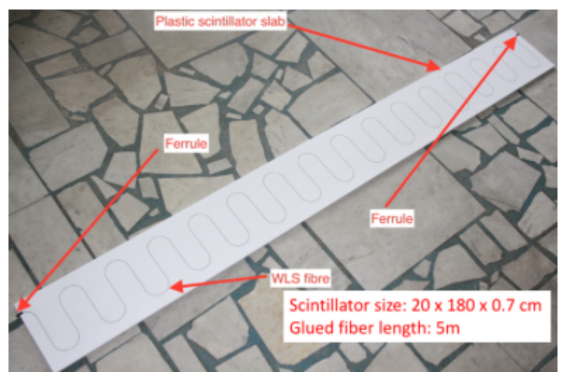

Figure 15: Left :Side-MRD module. Right: Scintillator bar of the Side-MRD modules.

Scintillators for the Side-MRD modules had been assembled at INR in Russia, and shipped to Japan in July 2017. The light yield for each scintillator was measured with cosmic rays at INR and at YNU in Japan after delivery. Parameters measured at the center of the counter were : the light yields LY_1 and LY_2 at both ends, the light yield asymmetry between the ends calculated as $100\% \times \frac{LY_1 - LY_2}{LY_1 + LY_2}$. After tests at INR we selected 324 counters from measured 332 ones with the mean light yield of 45 p.e./MIP (LY_1+ LY_2) and the asymmetry value less than 10 % . The measuremens at YNU yielded the average total light yield of about 40 p.e./MIP which varies in range from 32 to 50 p.e/MIP (Fig. 16 (left)). Only two counters showed relatively high asymmetry close to 25 % as shown in Fig. 16 (right). Using the results of the quality assurance test we selected 320 scintillator counters for the Side-MRD modules.

We also measured the time resolution for a combination of four counters piled each on another one. The average result for four counters is $\sigma_T = 1.04$ ns. The resolution of combination of 2, 3, 4 counters is measured to be 0.79 ns, 0.66 ns and 0.58 ns, correspondently.

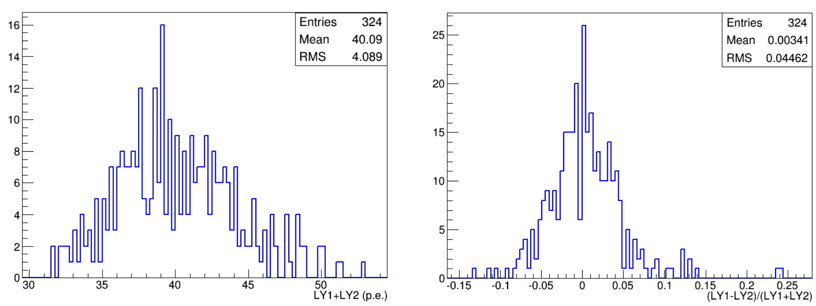

Figure 16: Total light yield distribution (left) and light yield assymetry (right) measured at YNU.

Construction of Side-MRD modules will be done from November 2017 at Yokohama National University, then they will be transported to J-PARC and will be installed at B2 floor of the T2K near detector hall.

Same electronics as the WAGASCI modules (see Sec. 2.1.2) are used for the Side-MRD modules.

3 Physics goals

We will measure the differential cross section for the charged current interaction on H_2O and Hydrocarbon(CH)). The water-scintillator mass ratio of the Wagasci module is as high as 5:1 and the high purity measurement of the cross section on H_2O is possible. One experimental option is to remove water from one of the two Wagasci modules. The water-out WAGASCI module will allow to measure pure-CH target interactions with very low momentum-threshold for protons. It will also benefit to subtract the background from interaction with scintillator in the water target measurement. Another option is to add the T2K proton module which is fully made of plastic scintillators. It will allow the high statistics comparison of cross section between H_2O and CH and also comparison with the ND280 measurement. The actual configuration will be optimized with detailed MC simulation by 2018 Summer.

Our setup allows the measurements of inclusive and also exclusive channels such as 1-μ, 1-$\mu 1p$, 1-$\mu 1\pi \pm np$ samples, former two of which are mainly caused by the quasi-elastic and 2p2h interaction and the latter is mainly caused by resonant or coherent pion production and deep elastic scattering. In general, an accelerator produced neutrino beam spectrum is wide and the energy reconstruction somehow rely on the neutrino interaction model. Therefore, recent neutrino cross section measurement results including those from T2K are given as a flux-integrated cross section rather than cross sections as a function of the neutrino energy to avoid the model dependency. We can provide the flux-averaged cross section. In addition, by combining our measurements with those at ND280, model-independent extraction of the cross section for narrow energy region becomes possible. This method was demonstrated in [1] and also proposed by P** (NUPRISM).

3.1 Expected number of events

Expected number of neutrino events after the event selections is evaluated with Monte Carlo simulations as we will discuss in Section 5. In the neutrino-mode, 4.2×10^3, 1.1×10^3 and 3.8×10^3 CC neutrino events are expected in the water-in WAGASCI module, the water-out WAGASCI module and the INGRID proton module after the selections with 0.5×10^{21} POT, and its purities are 78.0 %, 97.5 % and $\sim 98\%$. In the antineutrino-mode, 1.7×10^3, 0.4×10^3 and 1.5×10^3 CC antineutrino events are expected in the water-in WAGASCI module, the water-out WAGASCI module and the INGRID proton module after the selections with 0.5×10^{21} POT, and its purities are 59.5 %, 74.4 % and $\sim 74\%$.

Statical errors of flux integrated CC-inclusive neutrino cross section measurements on H_2O (full acceptance) and CH targets (forward acceptance) will be 1.5 % and 1.6 % with 0.5×10^{21} POT in the neutrino-mode. Statical errors of flux integrated CC-inclusive antineutrino cross section measurements on H_2O (full acceptance) and CH targets (forward acceptance) will be 2.4 % and 2.5 % with 0.5×10^{21} POT in the antineutrino-mode.

Statical errors of flux integrated H_2O to CH CC-inclusive neutrino cross section ratio measurement will be 3.1 % (full acceptance) and 2.3 % (forward acceptance) with 0.5×10^{21} POT in the neutrino-mode. Statical errors of flux integrated H_2O to CH CC-inclusive antineutrino cross section ratio measurement will be 5 % (full acceptance) and 3.7 % (forward acceptance) with 0.5×10^{21} POT in the antineutrino-mode.

3.2 Pseudo-monochromatic beam by using different off-axis fluxes

The off-axis method gives narrower neutrino spectrum, and the peak energy is lower for larger off-axis angle. There still remains high energy tail mainly due to neutrinos from

Kaon decay. The off-axis angle of the Wagasci location is 1.5 degree and different from the ND280 2.5 degree. Top two plots of Fig. 17 show the energy spectra of fluxes and neutrino interaction events at these two different location. The high energy tail of ND280 flux can be somehow subtraction by using the Wagasci measurement. The low energy part of the Wagasci flux can be also subtracted by using the ND280 measurement. Bottom two plots of Fig. 17 demonstrate this method. We can effectively get two fluxes, from 0.2 GeV to 0.9 GeV and 0.6 GeV and 2 GeV and measure flux-integrated cross section for these two fluxes.

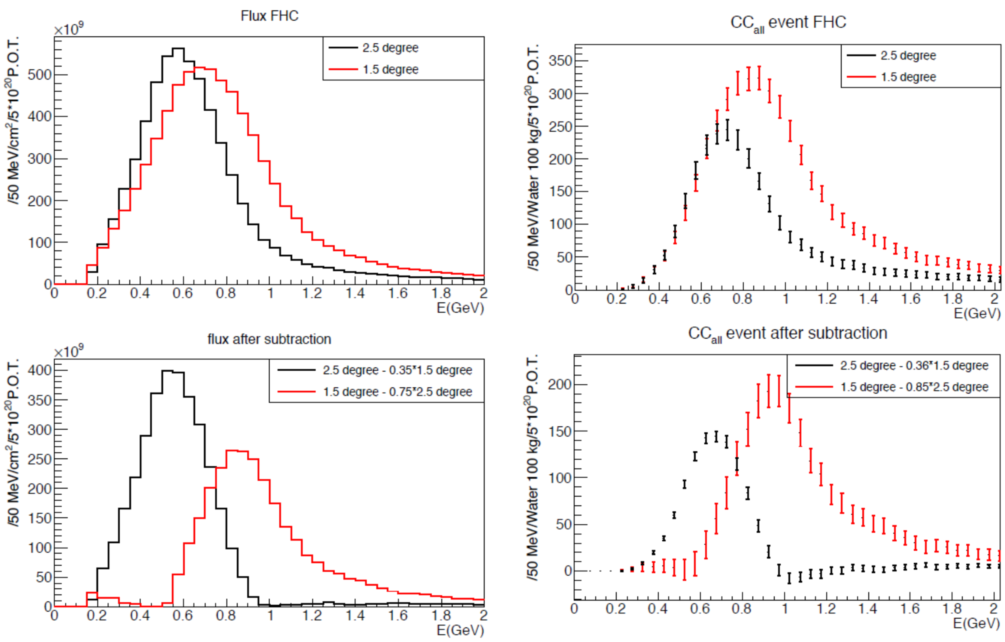

Figure 17: Energy spectra obtained by using different off-axis angle fluxes. Top two plots show the fluxes(left) and spectra of interaction events (right) for ND280 (off-axis 2.5 degree) and Wagasci (off-axis 1.5 degree). Bottom two plots show the fluxes (left) and spectra of interaction events (right) obtained by subtraction of fluxes at ND280 and Wagasci. The error bar is for the statistical error and those in the bottom right plot is obtained assuming the statistical error for ND280 measurement is much smaller than that of Wagasci experiment.

Statical errors of flux integrated CC-inclusive neutrino cross section measurements on H_2O (forward acceptance) and CH targets (forward acceptance) with the pseudo-monochromatic beam will be 2 % and 1.9 % with 0.5×10^{21} POT in the neutrino-mode. Statical errors of flux integrated CC-inclusive antineutrino cross section measurements on H_2O (forward acceptance) and CH targets (forward acceptance) with the pseudo-monochromatic beam will be 3 % and 2.8 % with 0.5×10^{21} POT in the neutrino-mode.

3.3 Subjects Wagasci can contribute

In T2K experiment, neutrinos interact with bound nucleons in relatively heavy nuclei (Carbon and Oxygen), so the cross-section is largely affected by nuclear effects. The nuclear effects are categorized as nucleons' momentum distribution in nucleus, interactions with correlated pairs of nucleons in nucleus (two particles-two holes, 2p2h), collective nuclear effects calculated with Random Phase Approximation (RPA) and final state interactions (FSI) of secondary particles in the nuclei after the initial neutrino interactions.

The 2p2h interactions mainly happen through Δ resonance interactions following a pion-less decay and interactions with a correlated nucleon pair. The 2p2h interactions are observed in electron scattering experiments [6] where the 2p2h events observed in the gap between Quasi-Elastic region and Pion-production region as shown in Fig. 18. Neutrino experiments also attempt to measure the 2p2h interactions, but separation of the QE peak and the 2p2h peak is more difficult because transferred momentum (p) and energy (w) are largely affected by neutrino energies which cannot be determined event-by-event in the wide energy spectrum of the accelerator neutrino beam. Our model-independent narrow neutrino spectra extracted from combined analyses of our data and ND280 data are ideal for searching the 2p2h interaction because clearer separation of the QE peak and the 2p2h peak is expected. Another way to observe the 2p2h interaction is direct measurement of proton tracks in CC0π sample with low detection threshold and full acceptance. Fig. 19 shows proton multiplicities after FSI in CCQE events and 2p2h events, and Fig. 20 shows opening angles among two proton tracks in the same samples. The water-out Wagasci can provide good sample for the 2p2h interaction search because its low density medium enables the detection of low momentum protons in addition to the full acceptance.

The corrections from collective nuclear effects calculated by RPA as a function of Q^2 are shown in Fig. **??**. The Q^2 dependence of the correction can be tested by measuring angular distribution of muons in CC1-μ and CC1-$\mu 1p$ events. The uncertainties of the corrections in low (high) Q^2 regions can be constrained by observing the events with a forward-going (high-angle) muon, so it is essential to measure muon tracks with full acceptance.

T2K experiment is starting to use ν_e CC1π events for its CP violation search to increase the statistics. One of the biggest uncertainty of the CC1π sample comes from the final state interactions of pions in the nuclei after the initial neutrino interactions because they change the multiplicity, charge and kinematics of the pions. The multi-pion production events can be migrated into the CC1π sample due to the FSIs, and they become important backgrounds. We can constrain the uncertainties from the pion FSIs by measuring pion rescattering in the detector and pion multiplicity in ν_μ CCnπ sample with low detection threshold and full acceptance for pion tracks. The water-out WAGASCI can provide good sample for the pion FSI studies because its low density medium enables the detection of low momentum pions in addition to the full acceptance.

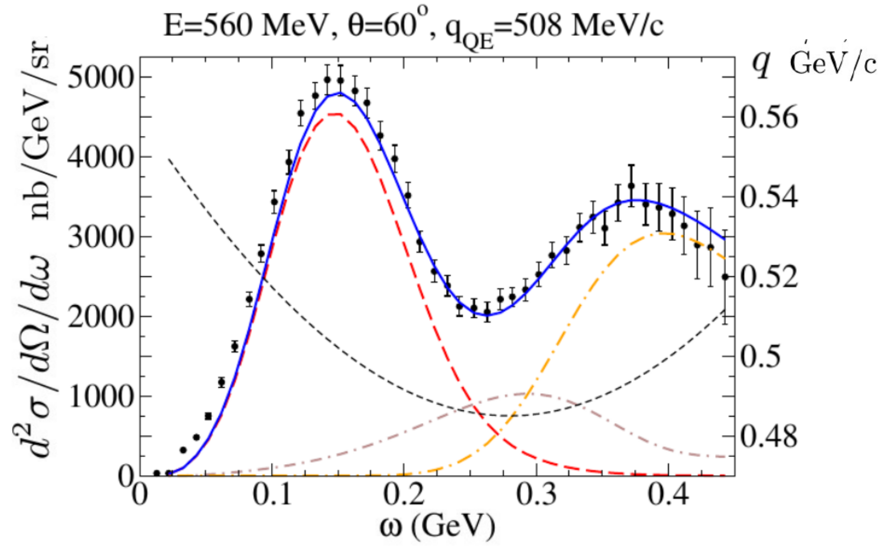

Figure 18: Comparison of inclusive ^{12}C(e,e') cross sections and predictions of the QE-SuSAv2 model (long-dashed red line), 2p-2h MEC model (dot-dashed brown line) and inelastic-SuSAv2 model (long dot-dashed orange line) (from Ref. [6]). The sum of the three contributions is represented with a solid blue line. The q dependence with w is also shown (short-dashed black line.)

4 Status of J-PARC T59 experiment

We had submitted a proposal of a test experiment to J-PARC in April 2014 to test a new detector with a water target, WAGASCI, at the neutrino monitor hall, and the proposal was approved as J-PARC T59. The project contains the side and downstream muon range detectors as well.

The first WAGASCI module has been constructed in 2016 and installed at the on-axis position in front of the T2K INGRID detector for the commissioning and the first cross section measurement as a part of the T2K experiment. The INGRID electronics boards are used to read the signal. The light yield measured with muons produced by the interaction of neutrinos in the hall wall, shown in Fig. 21, is sufficiently high to get good hit efficiency. A track search algorithm based on the cellular automaton has been developed using the software tools by the T2K INGRID. Examples of observed events are shown in Fig. 22 The tracking efficiency in 2-dimensional projected plane was evaluated by comparing the reconstructed track in the WAGASCI module and the INGRID module and shown in Fig.23. Note that that the tracking efficiency for high angle ($> 70\,\mathrm{deg}$) is not evaluated because of the acceptance of the INGRID module, not because of the limitation

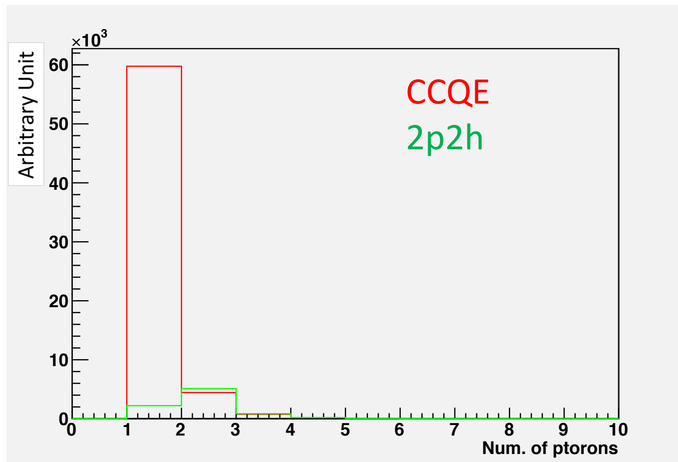

Figure 19: Proton multiplicities after FSI in CCQE events and 2p2h events.

of the WAGASCI module.

In 2017 Autumn, the construction of the second WAGASCI module and the dedicated electronics board were completed. The module and the electronics were install to the B2 floor together with the T2K proton module and the INGRID module as shown in Fig. 24. The proton module is to be used as the entering muon veto and also for the comparison of interaction between CH and Water. The INGRID module is for the temporary muon detector with limited acceptance for this period. The detector was commissioned and is in operation to take data with the antineutrino beam during the T2K beam time from October.

The production of the components of the side muon range detectors has been completed and now the detectors are being assembled at the Yokohama National University. These detectors will be installed sometime from January to June, 2018 when T2K is not running.

The Baby MIND detector was transported from CERN to Japan in December, 2017. It will be installed and commissioned in Jan.-Feb. 2018 and T59 will take the neutrino-induced muon data in April and May.

5 MC studies

5.1 Detector simulation

Expected number of neutrino events in the water-in Wagasci detector is evaluated with Monte Carlo simulations. Neutrino beam flux at the detector location is simulated by

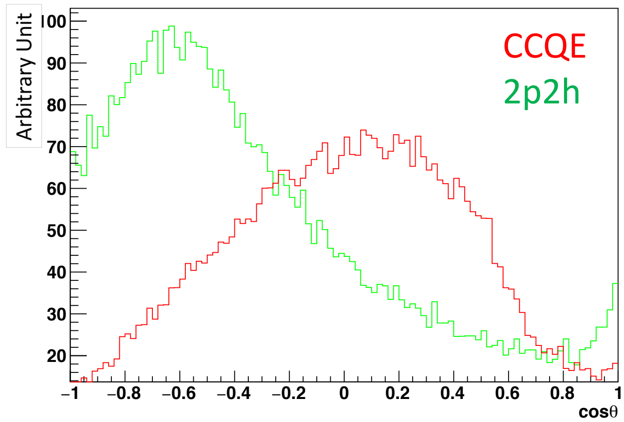

Figure 20: Opening angles among two proton tracks after FSI in CCQE events and 2p2h events.

T2K neutrino flux generator, JNUBEAM, neutrino interactions with target materials are simulated by a neutrino interaction simulator, NEUT, detector responses are simulated using GEANT4-based simulation. The neutrino flux at the detector location, 1.5 degrees away from the J-PARC neutrino beam axis, is shown in Figure 4, and its mean neutrino energy is around 0.68 GeV.

5.1.1 Detector geometry

The detector geometry in the GEANT4-based simulation is slightly different from the actual detector as shown in Fig. 25. The active neutrino target region consists of four Wagasci modules, and each Wagasci detector has the dimension with 100 cm $\times$ 100 cm in the x and y directions and 50 cm along the beam direction. Two Side-MRD modules is installed at both sides of the Wagasci modules, and each Side-MRD module consists of ten iron plates whose dimension is 3 cm (thickness) $\times$ 200 cm (height) $\times$ 320 cm (width). The distance between the Side-MRD modules and Wagasci modules is 80 cm. The downstream-MRD equivalent to the Baby-MIND is installed at the downstream of the Wagasci modules. The downstream-MRD consists of thirty iron plates whose dimension is 3 cm (thickness) $\times$ 200 cm (height) $\times$ 400 cm (width). The distance between the downstream-MRD modules and Wagasci modules is 80 cm.

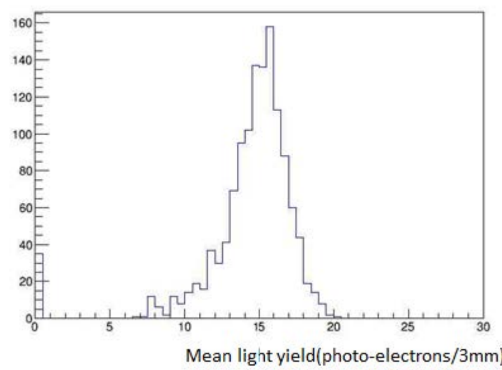

Figure 21: Light yield for muons produced by the interaction of neutrinos in the hall wall. Average light yields for each channel are plotted.

5.1.2 Response of detector components

The energy deposit inside the scintillator is converted into the number of photons. The effects of collection and attenuation of the light in the scintillator and the WLS fiber are simulated, and the MPPC response is also taken into account. The light yield is smeared according to statistical fluctuations and electrical noise.

5.2 Track reconstruction

To select neutrino interaction from the hit patterns, a track reconstruction algorithm is developed. The flow of the track reconstruction is as follows.

1. Two-dimensional track reconstruction in each sub-detectors
2. Track matching among the sub-detectors
3. Three -dimensional track reconstruction

Add explanation about two-dim reco, track matching and three-dim reco here.

5.3 Event selection

First, the events with the track which starts in 5 cm from the wall of the Wagasci module are rejected to remove the background from the outside.

Second, to reject backgrounds from NC and neutral particles, the longest tracks are required to penetrate more than one (five) iron plates in Side-MRD modules (Baby-MIND).

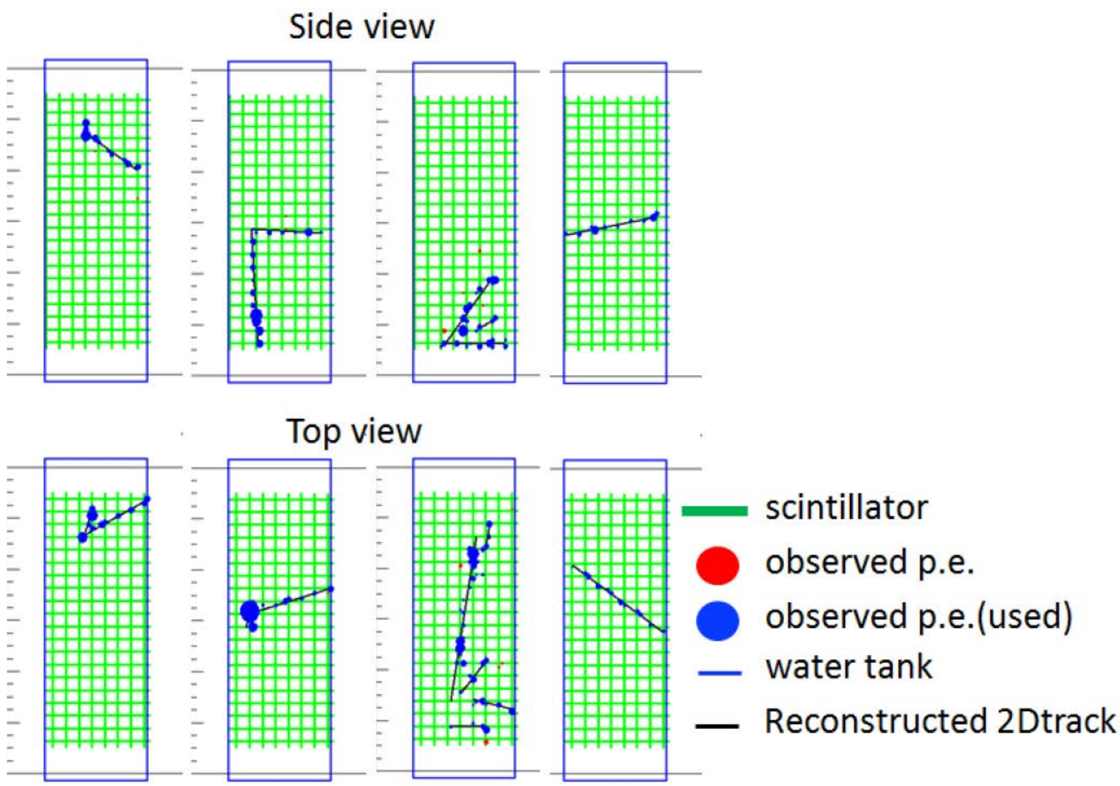

Figure 22: Example event displays of the WAGASCI module at on-axis. The reconstructed tracks are overlaid.

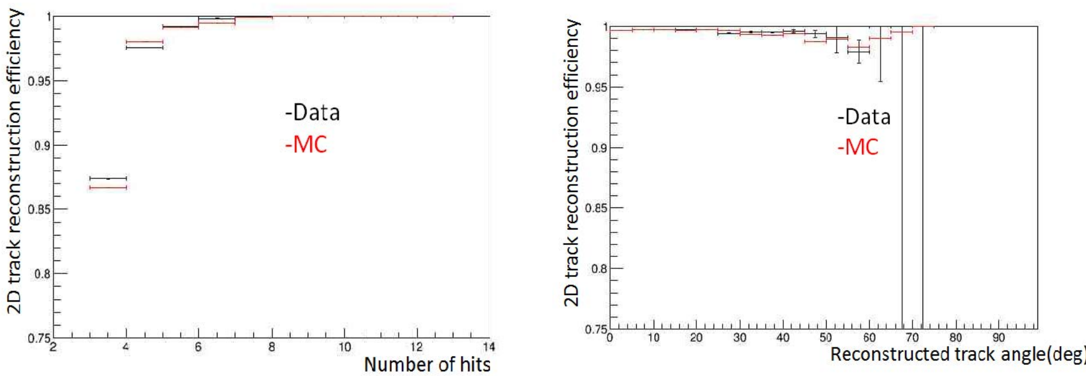

Figure 23: 2D track reconstruction efficiency as a function of number of hits (left) and track angle (right). Here the track angle is the one reconstructed by the INGRID module.

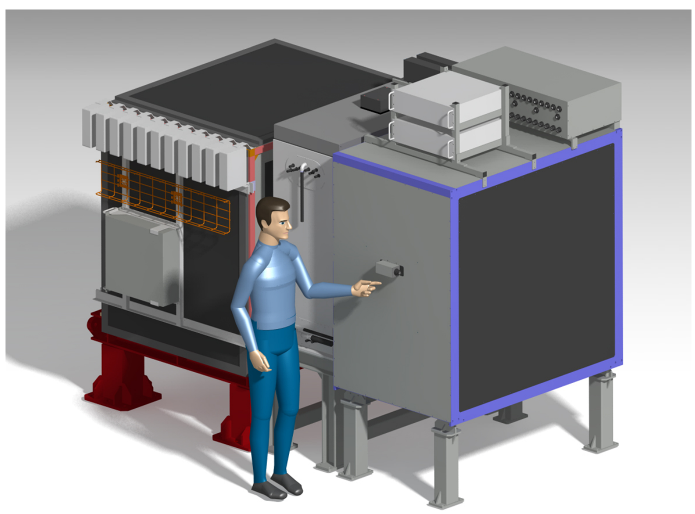

Figure 24: J-PARC T59 detector configuration in October 2017.

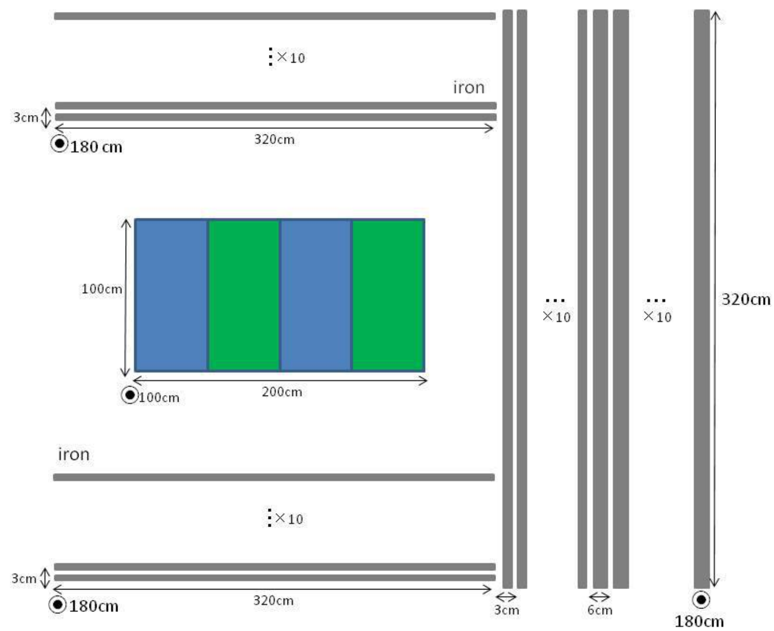

Figure 25: Geometry of the detectors in the Monte Carlo simulation.

Then, in order to measure muon momentum, the longest tracks are required to stop in MRDs (Side-MRD modules and Baby-MIND) or penetrate all iron plates.

Table 1 and 2 show numbers of the selected events in one water-in Wagasci module after each event selection in neutrino-mode and antineutrino-mode respectively. As for the neutrino-mode, 8478 CC events are expected with 1×10^{21} POT, and the purity is 78.0 %. The main background for the neutrino-mode is the neutrino interactions in the scintillators inside the Wagasci detector. As for the antineutrino-mode, 3331 CC events are expected with 1×10^{21} POT, and the purity is 59.5 %. The main background for the antineutrino-mode is the wrong sign contamination from ν_μ events and the antineutrino interactions in the scintillators inside the Wagasci detector.

Table 3 and 4 show numbers of the charged-current events in the water-in Wagasci module after all event selection with a classification based on interactions at a vertex with $1{\times}10^{21}$ POT in neutrino-mode and antineutrino-mode respectively.

Table 5 and 6 show numbers of the charged-current events in one water-in Wagasci module after all event selection with a classification based on particles after final state interactions with $1{\times}10^{21}$ POT in neutrino-mode and antineutrino-mode respectively.

Figure 26 and 27 show the reconstructed angles of the longest tracks in the selected events in the neutrino-mode and the anti-neutrino mode respectively. Figure 28, 29 30

Table 1: Expected number of the neutrino-candidate events in one water-in Wagasci module with 1×10^{21} POT in neutrino-mode.

Cut	CC	NC	Scinti Bkg.	Total
Reconstructed	18093.2	699.7	4698.3	23491.2
FV	15150.8	588.4	3934.8	19673.9
Pene. iron	11264.3	237.3	2875.4	14377.0
Stop/Penetrate MRDs	8478.2	214.0	2173.1	10865.2
after all cuts	78.0 %	2.0 %	20.0 %	100 %

Table 2: Expected number of the antineutrino-candidate events in one water-in Wagasci module with 1×10^{21} POT in antineutrino-mode.

Cut	CC	NC	Scinti Bkg.	Wrong sign bkg	Total
Reconstructed	6499.7	107.3	2234.4	2330.8	11172.1
FV	5457.9	89.3	1873.5	1946.6	9367.1
Pene. iron	4172.3	30.8	1440.9	1560.6	7204.6
Stop/Penetrate MRDs	3331.5	28.5	1120.3	1121.2	5601.5
after all cuts	59.5 %	0.5 %	20.0 %	20.0 %	100 %

and 31 show the iron plane numbers in Side-MRD and Baby-MIND corresponding to the end points of the longest tracks in the selected events in the neutrino-mode and the anti-neutrino mode.

5.4 Cross section measurements on water

In the water target events, the background from interaction with scintillators has to be subtracted by using the measurement of the hydrocarbon target.

Table 3: Expected number of the charged-current events in the water-in Wagasci module after the event selections with 1×10^{21} POT in neutrino-mode with a classification based on interactions at a vertex.

CCQE	MEC	CCRes	CCDIS	Total
3716.3	747.0	2081.3	1132.3	7676.9
48.4 %	9.7 %	27.1 %	14.7 %	100 %

Table 4: Expected number of the charged-current events in the water-in Wagasci module after the event selections with 1×10^{21} POT in antineutrino-mode with a classification based on interactions at a vertex.

CCQE	MEC	CCRes	CCDIS	Total
2522.0	362.8	765.8	765.8	4416.4
hline 57.1 %	8.2 %	17.3 %	17.3 %	100 %

Table 5: Expected number of the charged-current events in one water-in Wagasci module after the event selections with 1×10^{21} POT in neutrino-mode with a classification based on particles after final state interactions.

CC0π	CC1π	CC2π	CCnπ	Total
5423.1	1684.3	242.9	701.1	8051.4
67.4 %	20.9 %	3.0 %	8.7 %	100 %

5.4.1 Charged current cross section measurement

6 Standalone WAGASCI-module performances

In the previous sections, the WAGASCI detector was studied using the Muon Range Detectors. In this section, the standalone abilities of WAGASCI module are presented. Using the WAGASCI configuration presented in Section 5, we have evaluated that only 7% of the muons will be stopped in one of the WAGASCI modules. THowever, this proportion increases to 53% for pions and 73% for protons produced by neutrino interactions at 1.5° off-axis. Figure 32 shows the momentum distribution of these daughter particles as well as for the sub-sample stopped in one of the WAGASCI modules. Therefore, the study of the standalone abilities of the WAGASCI module in this section are dominantly motivated by:

- the accurate measurement of the neutrino interaction final states. Though most of the muons will be reconstructed and identified in the MRDs, the hadronic particles will

Table 6: Expected number of the charged-current events in one water-in Wagasci module after the event selections with 1×10^{21} POT in antineutrino-mode with a classification based on particles after final state interactions.

CC0π	CC1π	CC2π	CCnπ	Total
2529.3	520.0	37.9	96.0	3183.2
79.5 %	16.3 %	1.2 %	3.0 %	100 %

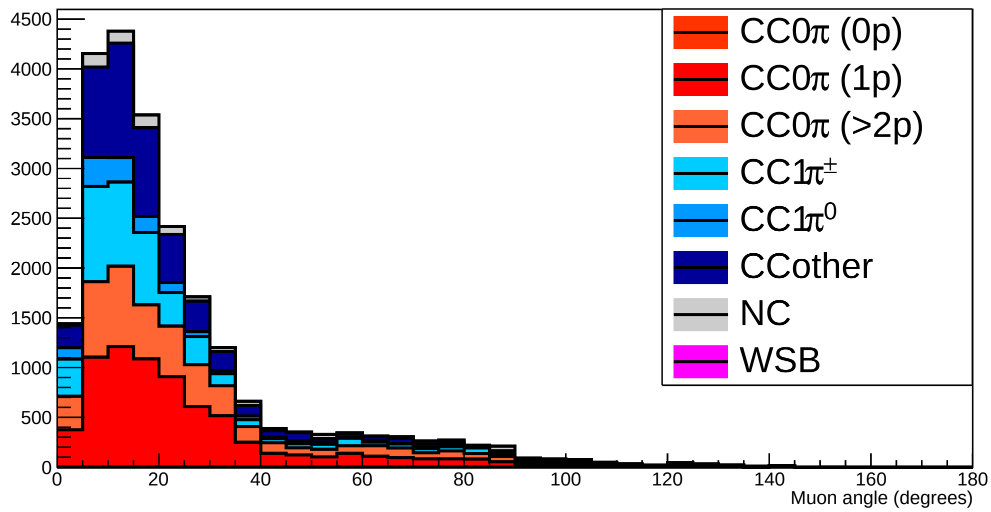

Figure 26: The reconstructed angles of the longest tracks in the selected events in the neutrino-mode.

predominantly stops in one WAGASCI module. One has therefore to rely exclusively on the WAGASCI module information alone to reconstruct, identify and measure the momentum of pions or protons.

- the coverage of the MRDs is not 4π. Using the WAGASCI module information can therefore help to constraint the particles that exits the WAGASCI module but do not geometrically enters any MRD.

- the particle identification of low momenta muons $p_\mu < 300$ MeV/c that will leave only few hits in the MRD. Using the WAGASCI module information will clearly enhance the particle identification.

This study is based on an original study done for the ND280 upgrade target, with some modifications. Though the cell size is similar to the WAGASCI configuration presented in Section 5, the external dimensions are different ($186.4 \times 60 \times 130$ cm^3). Whenever the results are presented with this external size and this parameter is likely to impact the result, it will be mentioned.
Note that in this section, a simplified reconstruction algorithm presented in Section 6.1 is used. The fiducial volume is chosen accordingly as the inner cube of the module which surfaces are distant of $4 \times$ scintillator space $= 10$ cm from the module external surfaces.

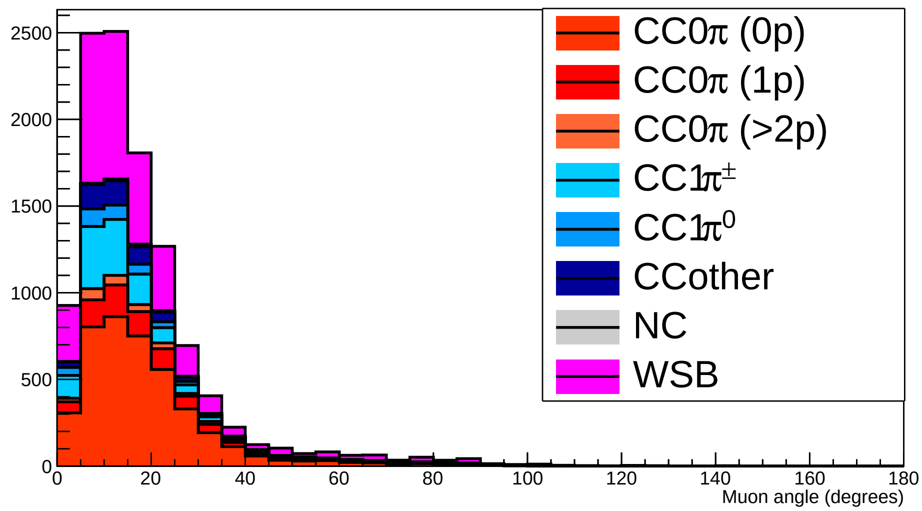

Figure 27: The reconstructed angles of the longest tracks in the selected events in the antineutrino-mode.

The neutrino interactions are simulated using NEUT v5.3.2. The NEUT input neutrino flux is estimated using JnuBeam v13a and assuming the detector to be located at 1.5° off-axis, as in Section 5. Note that the event reconstruction efficiency as a function of true neutrino energy might be changed at 1.5°, due for example to different Q^2 distributions. For this reason, one has to note that the reconstruction results might slightly be changed from 2.5° and 1.5°. To avoid a similar change on the particle-only reconstruction efficiencies, they will be presented as a function of variables that completely characterize the particle kinematic state, *i.e.* its momentum and angle. Figure 33 shows the vertices distributions of the daughter particles of neutrinos interacting one standard WAGASCI water-module. In this section, we will show the detector reconstruction and particle identification in this phase space, both for leptonic and hadronic particles. We will finally show an empty WAGASCI module can highly enhance the ability to constrain the neutrino interaction final state which is critical to reduce the corresponding uncertainties.

6.1 Reconstruction algorithm

6.1.1 Description

For this section, an ideal "simulated" reconstruction is developed. A particle is reconstructed if:

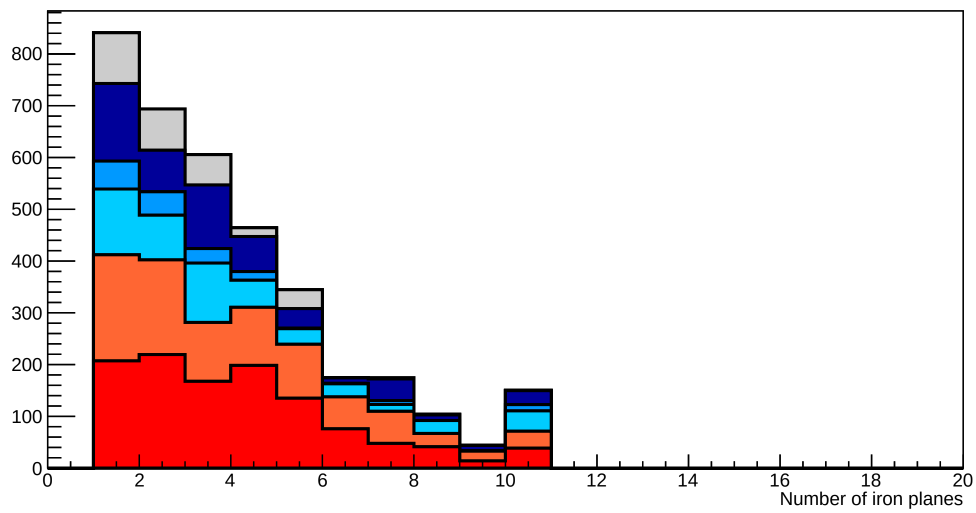

Figure 28: Iron plane numbers in Side-MRD corresponding to the end points of the longest tracks in the selected events in the neutrino-mode.

1. The particle is charged.
2. Lets at least one hit (energy deposit $>$ 2.5 photo-electron) in a scintillator.
3. The particle enters one TPC and let one hit in the tracker.
   Or

   - The particle should be long enough to be reconstructed by the detector in at least 2 out of 3 views (XZ, YZ, XY). The length criterion requires the particle to let at least 4 hits in the detector. In the “less favourable case” of pure longitudinal or tranverse going tracks, it represents a the track length of $L_{track} \geq 4 \times \text{scintillator space} = 10.0$ cm.
   - In the views where particles pass the length criterion, the particle shall not be superimposed with longer tracks in at least two views. The superposition criterion is estimated with the distance inter-tracks (DIT) which corresponds to the orthogonal distance between two tracks at the ending point of the shortest one (see Figure 34). For a track 1, the superposition criterion is tested with every longer tracks that starts at the same vertex. Let $\vec{p_1}$ the vector of track

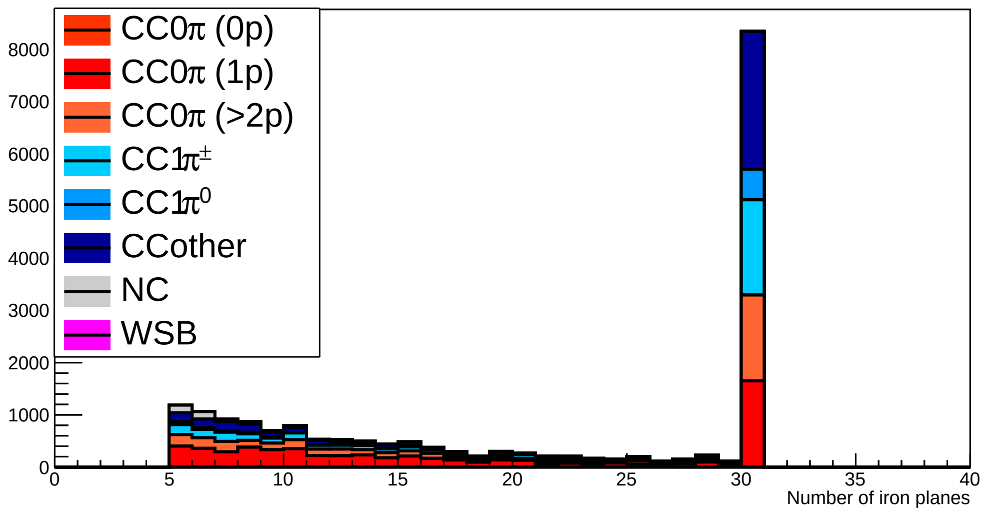

Figure 29: Iron plane numbers in Baby-MIND corresponding to the end points of the longest tracks in the selected events in the neutrino-mode.

1, and p_1^a its projections in the XZ, YZ and XY planes respectively for i=1,2,3. Note that these are projections in a 2D planes and not on a direction vector. In this case, the relative angle between the track 1 and a longer track 2 (of vector $\vec{p_2}$) in a view a is given by:

$$\cos\theta = \frac{\vec{p_1^a} \cdot \vec{p_2^a}}{||\vec{p_1^a}||||\vec{p_2^a}||} \tag{1}$$

and the distance inter track is given by:

$$\mathrm{DIT} = ||\vec{p_1^a}|| \sin\theta \tag{2}$$

The DIT should be higher than $4 \times$ scintillator width for the track 1 to be not superimposed with the track 2 in the view a, which also corresponds to 10.0 cm in the nominal configuration.

6.1.2 Performances

The particle-only reconstruction efficiencies and the reconstruction threshold in momenta are shown in Table 7. This threshold is defined as the maximal momentum for which the

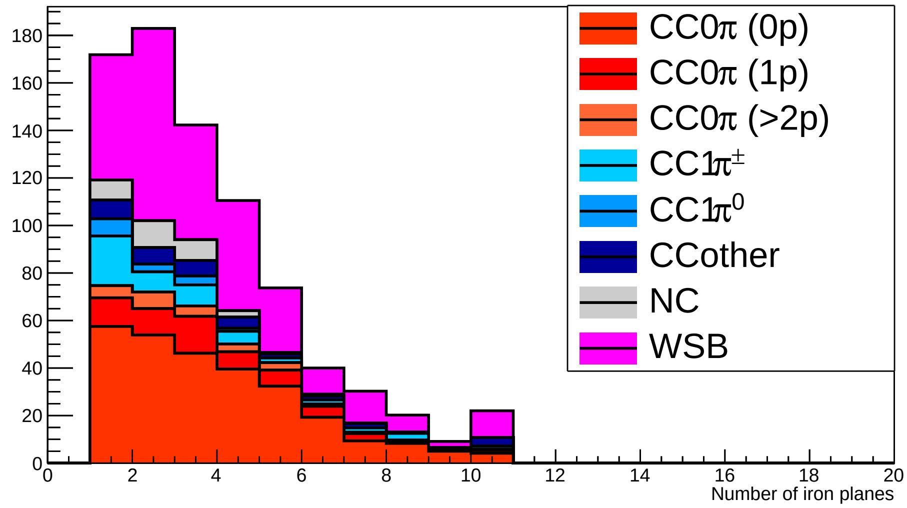

Figure 30: Iron plane numbers in Side-MRD corresponding to the end points of the longest tracks in the selected events in the antineutrino-mode.

reconstruction efficiency is smaller than 30%. The thresholds in muon and pion momenta are 150 MeV/c. Most of the muons are above this threshold (see Figure 33) which leads to a 79% reconstruction efficiency.

	μ	π	p
Reconstruction Efficiency	79%	52%	26%
Momentum threshold	150 MeV/c	150 MeV/c	550 MeV/c

Table 7: Reconstruction efficiency and momentum threshold for muons, pions and protons. The threshold is defined as the maximal momentum for which particles have a reconstruction efficiency smaller than 30%.

The lower pion and proton efficiencies (respectively 52% and 26%) are due to lower efficiencies for similar momenta than muons, coming from strong interactions as shown on Figures 35. Efficiencies of each particle type tend to decrease in the backward region due to particle lower momenta. However, for a fixed momentum value, the reconstruction efficiency is almost uniform which confirms the ability of the WAGASCI detector to reconstruct high angle tracks.

The reconstruction is thereafter tested on neutrino events. Table 8 summarizes the number of reconstructed events and efficiencies for each interaction type. As expected

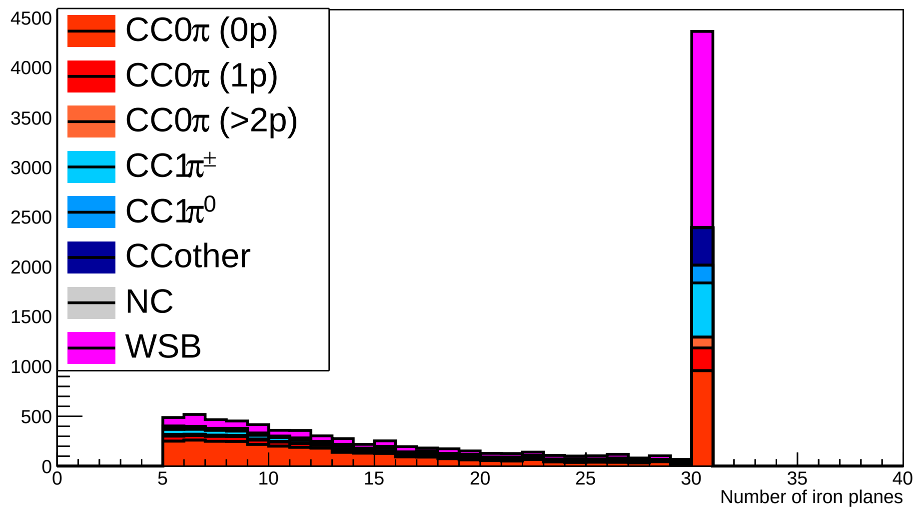

Figure 31: Iron plane numbers in Baby-MIND corresponding to the end points of the longest tracks in the selected events in the antineutrino-mode.

626 from the high muon reconstruction efficiency, the charged current interactions have reconstruction efficiencies $\geq 85\%$.

	CC0π	CC1π	CCOthers	NC	All
Reconstruction efficiency	85%	87%	91%	22%	68%

Table 8: Number of true interactions reconstructed. The purity and reconstruction efficiency of each true interaction is also shown.

627

628 The reconstruction efficiencies as a function of the neutrino energy and muon kinematics
629 are respectively shown on Figure 36 and 37.

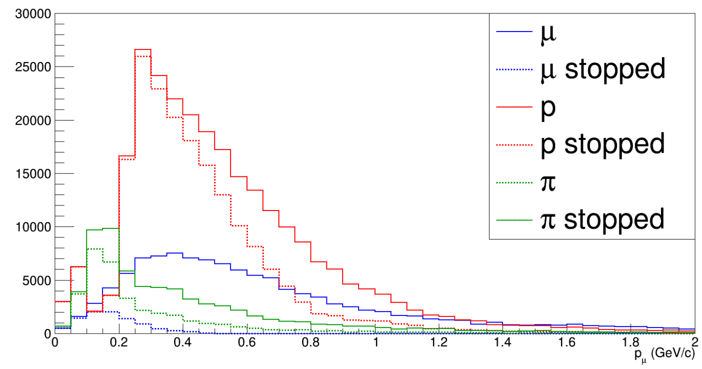

Figure 32: Momentum distribution of true particles in WAGASCI (plain) and corresponding distributions only for particles stopping into the WAGASCI module (dashed).

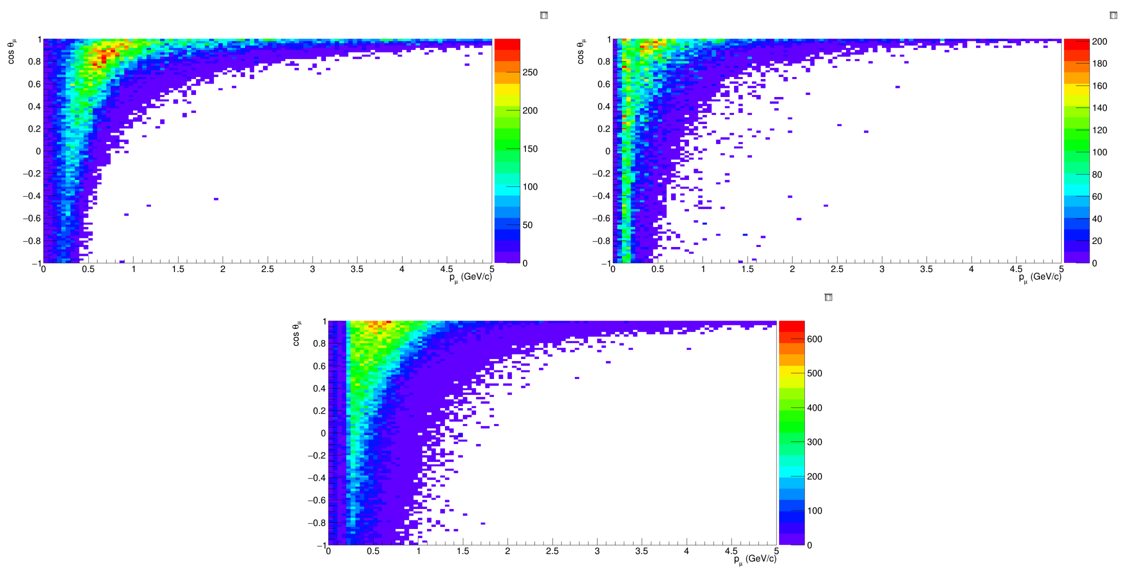

Figure 33: True number of muons (left), charged pions (right) and protons (bottom) in the two WAGASCI water-module as a function of the particles momenta and angles at 1.5°.

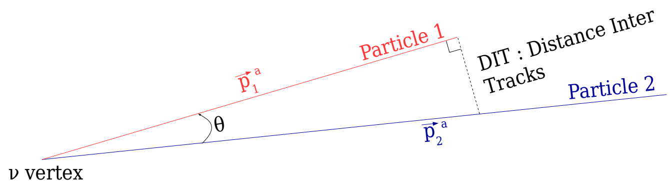

Figure 34: Definition of the distance inter tracks.

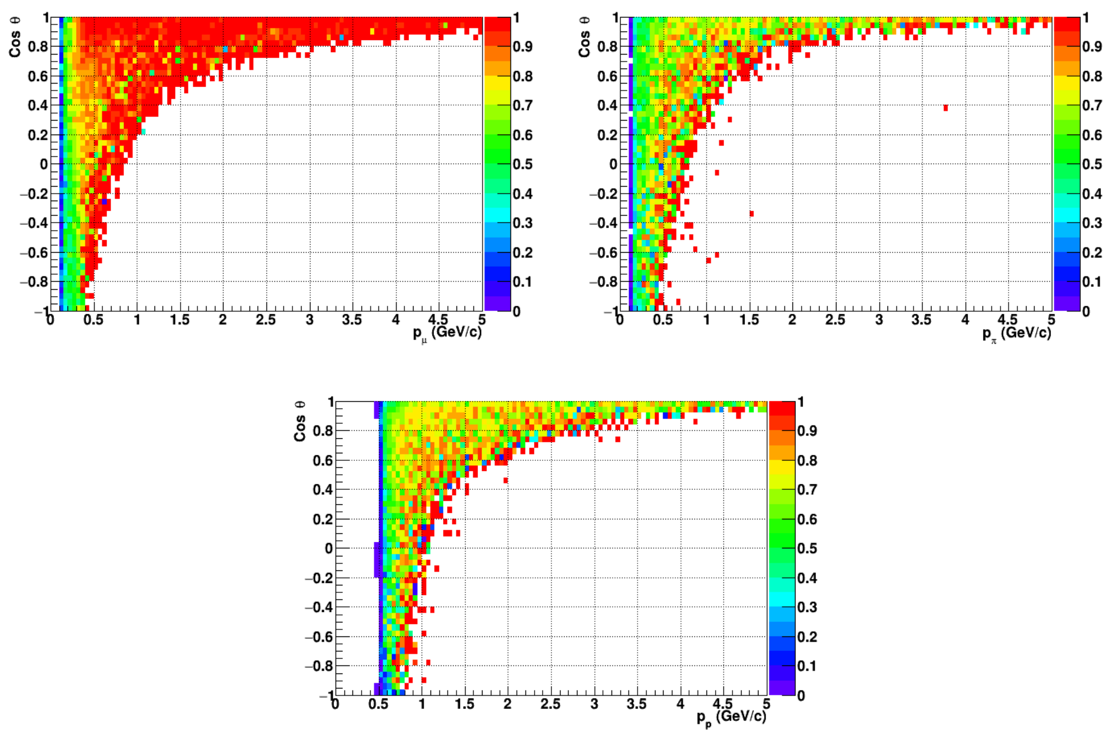

Figure 35: Reconstruction efficiency of muons (left), charged pions (right) and protons (bottom) in the WAGASCI water-module as a function of the particles momenta and angles.

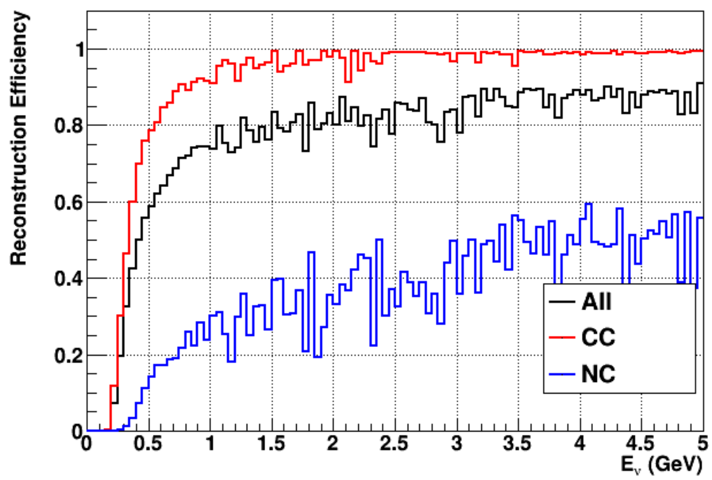

Figure 36: Reconstruction efficiency of all neutrino (black), CC (red) and NC (blue) interactions in the WAGASCI water-module as a function of the neutrino energy.

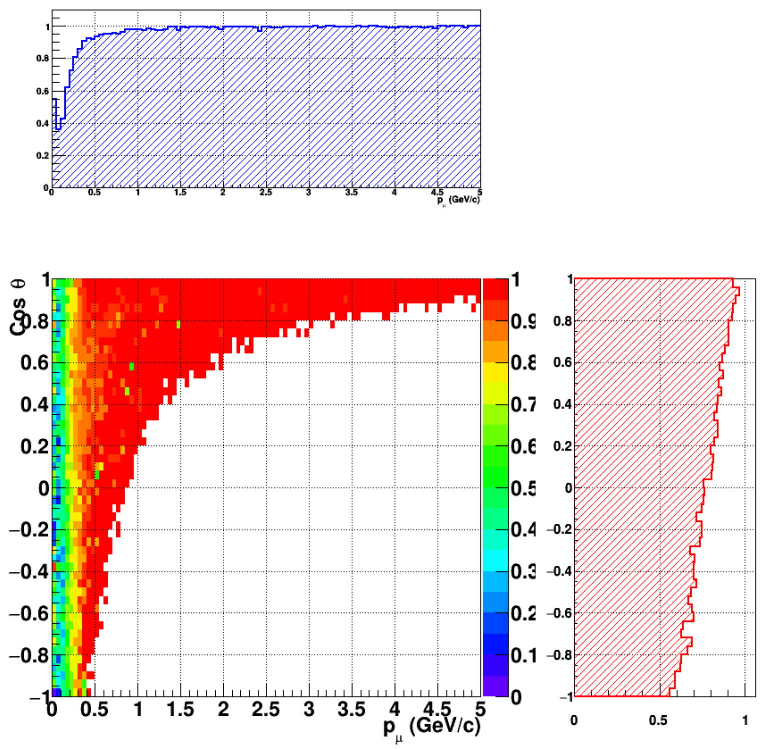

Figure 37: Reconstruction efficiency of CC interactions in the WAGASCI water-module as a function of the muon kinematic variables (momentum and angle).

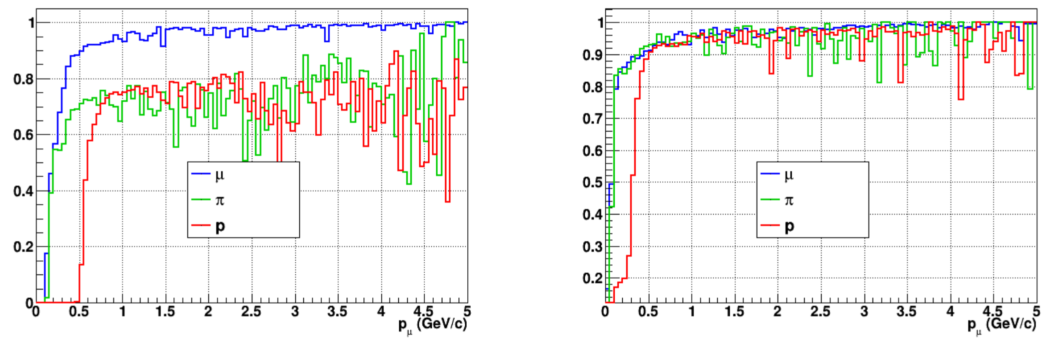

Figure 38: Reconstruction efficiency for muons, pions and protons in the water-in (left) and water-out (right) modules.

Note that a Particle Identification Algorithm has been also developed. It is based on the charge deposition of the particles in the scintillator, of the detection of a decay-electron. However, this information highly depends on the number of scintillator hit by a particle, which creates an important difference between a real WAGASCI module and the one used for the ND280-upgrade simulation. For this reason, the corresponding results will not be detailed here, but can be found in [**?**].

6.2 Background substraction: the water-out module

In the nominal configuration, 20% of the neutrino interactions occurs on scintillators (C_8H_8). This background should be removed in order to measure the neutrino interaction on the same target as Super-K, which suppress the differences in cross-section models. For this purpose, we propose to use a water-out module, where the water is replaced by air. The detector is therefore fully active and has a 3 mm spatial resolution (scintillator thickness) which create and ideal detector to reconstruct and identify hadrons, and study np-nh interactions. The counter-part is the difference in particle energy deposition between the water and this water-out module that will need to be corrected for. In this section, we present the capabilities of such a module, and the impact it can have on cross-section measurements for the neutrino community in genral and T2K in particular.
The same reconstruction and selection as the water-in module is applied. Figure 38 shows the comparison between the water-in and the water-out reconstruction efficiencies for muon, pions and protons. 90% of the muons and 87% of the pions are reconstructed, while 70% of the protons are even reconstructed. It allows to low down the proton threshold to 250 MeV/c (see Table 9).

As a consequence of tracking even low momenta particle, the reconstruction efficiency is uniform and almost maximal on the entire $\cos\theta_\mu$ phase space, as shown on Figure 39.

	μ	π	p
Reconstruction Efficiency	90%	87%	70%
Momentum threshold	50 MeV/c	50 MeV/c	250 MeV/c

Table 9: Reconstruction efficiency, proportions of μ-like and non μ-like and momentum threshold for muons, pions and protons in the empty module. The threshold is defined as the maximal momentum for which particles have a reconstruction efficiency smaller than 20%.

Since the fiducial mass represents 0.25 tons, the total number of events is divided by a factor of 3 compared to the water-in module. The water-out module offers interesting possibilities to study np-nh interaction since 70% of the protons are reconstructed. In the future, a possible separation as a function of the number of proton track will be studied. Morevover, we are currently pursuing the use of single and double transverse variables (cite Xianguo) to open new possibilities for separating np-nh from Final State Interactions, or for isolating the interactions on hydrogen from interactions on carbon in this module.

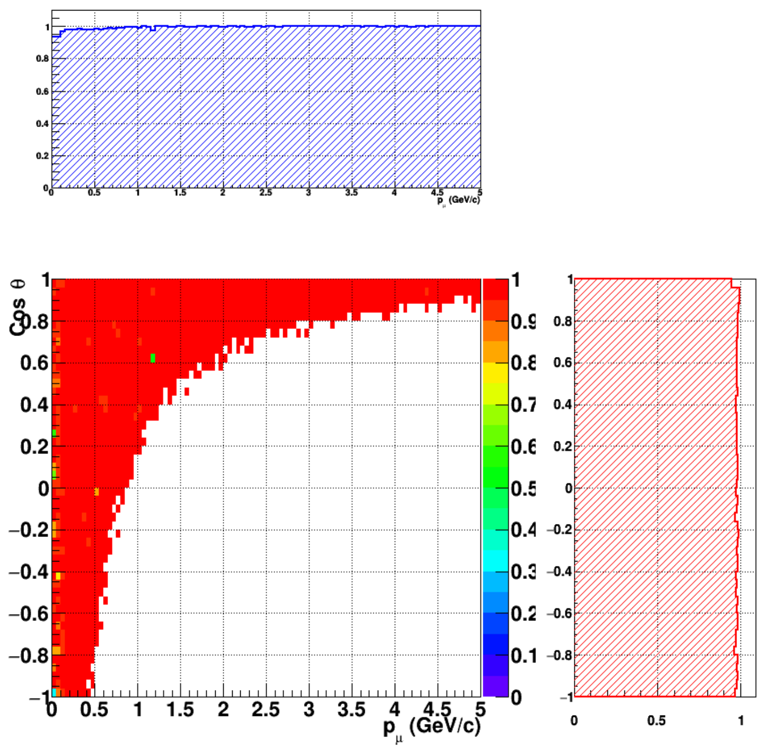

Figure 39: Reconstruction efficiency of CC interactions in the WAGASCI empty module as a function of the muon kinematic variables (momentum and angle).

7 Schedule

We would like to start a physics data taking from T2K beam time after the summer shutdown in 2018. By then, commissioning and tests of the detectors will be completed in J-PARC T59. The experiment can run parasitically with T2K, therefore we request no dedicated beam time nor beam condition as discussed in the following section.

Once the approved POT is accumulated, the WAGASCI modules will be removed from the experimental site, but we would like to keep the Baby-MIND and the Side-MRD modules on the B2 floor of the NM pit as common platforms of future neutrino experiments using the T2K neutrino beam.

8 Requests

8.1 Neutrino beam

The experiment can run parasitically with T2K, therefore we request no dedicated beam time nor beam condition. As data taking periods, we request the 'nominal' T2K one-year operation both for the neutrino beam and the antineutrino beam. The T2K has been requesting 0.9×10^{21} POT/year and actually accumulating about 0.7×10^{21} POT/year in recent years. For each year, starting from the Autumn, T2K is running predominantly in the neutrino mode or in the antineutrino mode. Our request is to have one-year neutrino-mode data and another one-year antineutrino mode data assuming that the POT for the fast extraction in each year is more than 0.5×10^{21} POT.

8.2 Equipment request including power line

We request the followings in terms of equipment on the B2 floor:

- Site for the WAGASCI modules, Side-MRD modules and BabyMIND and their electronics system on the B2 floor of the near detector hall (Fig. 3).
- Anchor points (holes) on the B2 floor to secure the WAGASCI modules, Side-MRD module and Baby-MIND (Fig. **??**)
- Power line for the magnets in Baby-MIND: 400 V tri-phase 48-to-62 Hz, capable of delivering 12 kW.
- Electricity for electronics and water circulation system, 3 kW, standard Japanese electrical sockets.

    1. Online PCs: 2.1 kW
    2. Electronics: 0.7 kW
    3. Water sensors: ?

- Air conditioner for cooling heat generation at Baby-MIND magnets, online PCs and electoronics
- Beam timing signal and spill information
- Network connection

8.2.1 Baby MIND Equipment request including power line

We request the following in terms of equipment on the B2 floor:

- Site for the Baby MIND detector and its electronics systems on the B2 floor of the near detector hall.
- Anchor points (holes) on the B2 floor to secure the 9 support frames, of order 4 holes per frame, detailed floor plans to be communicated in a separate document.
- Power line for the magnet: 400 V tri-phase 48-to-62 Hz, capable of delivering 12 kW. We have a wish for the magnet power line to be installed and available to us by beginning of March 2018.
- Electricity for electronics, 1 kW, standard Japanese electrical sockets.
- Beam timing signal and spill information
- Network connection

The infrastructure for much of the above exists already, and will be shared in part with the WAGASCI experiment. Exceptions are the power line for the magnet and holes in the B2 floor to anchor the detector support structures.

9 Conclusion

References

[1] K. Abe et al. Measurement of the muon neutrino inclusive charged-current cross section in the energy range of 13 GeV with the T2K INGRID detector. *Phys. Rev.*, D93(7):072002, 2016.

[2] M. Antonova et al. Baby MIND Experiment Construction Status. In *Prospects in Neutrino Physics (NuPhys2016) London, London, United Kingdom, December 12-14, 2016*, 2017.

[3] K. Nitta et al. The k2k scibar detector. *Nucl. Instrum. Meth. A*, 535:147, 2004.

[4] F. Magniette F. Gastaldi, R. Cornat and V. Boudry. A scalable gigabit data acquisition system for calorimeters for linear collider. *proceedings of TIPP2014*, page PoS 193, 2014.

[5] J. Fleury, S. Callier, C. de La Taille, N. Seguin, D. Thienpont, F. Dulucq, S. Ahmad, and G. Martin. Petiroc and Citiroc: front-end ASICs for SiPM read-out and ToF applications. *JINST*, 9:C01049, 2014.

[6] M. B. Barbaro J. A. Caballero T. W. Donnelly G. D. Megias, J. E. Amaro. Inclusive electron scattering within the susav2 meson-exchange current approach. *Phys. Rev. D*, 94:013012, 2016.

[7] Yu. G. Kudenko, L. S. Littenberg, V. A. Mayatsky, O. V. Mineev, and N. V. Ershov. Extruded plastic counters with WLS fiber readout. *Nucl. Instrum. Meth.*, A469:340–346, 2001.

[8] O. Mineev, Yu. Kudenko, Yu. Musienko, I. Polyansky, and N. Yershov. Scintillator detectors with long WLS fibers and multi-pixel photodiodes. *JINST*, 6:P12004, 2011.

[9] Etam Noah et al. Readout scheme for the Baby-MIND detector. *PoS*, PhotoDet2015:031, 2016.

[10] Omega. Spiroc 2 user guide. 2009.